RESEARCH ARTICLE | SEPTEMBER 11 2023

An open-source anisotropic $k - \varepsilon - v^2 - f$ model for turbulent viscoelastic duct flows

M. McDermott ; T. A. E. Riou ; P. R. Resende ; M. C. T. Wilson ; A. M. Afonso ; G. de Boer

Physics of Fluids 35, 095116 (2023)
https://doi.org/10.1063/5.0159668

Physics of Fluids ARTICLE pubs.aip.org/aip/pof

An open-source anisotropic $k-\varepsilon-v^2-f$ model for turbulent viscoelastic duct flows

Cite as: Phys. Fluids **35**, 095116 (2023); doi: 10.1063/5.0159668
Submitted: 25 May 2023 · Accepted: 8 August 2023 ·
Published Online: 11 September 2023

M. McDermott,[1,a] T. A. E. Riou,[1,b] P. R. Resende,[2,c] M. C. T. Wilson,[1,d] A. M. Afonso,[3,e] and G. de Boer[1,f]

AFFILIATIONS

[1]School of Mechanical Engineering, University of Leeds, Woodhouse Lane, Leeds LS2 9JT, United Kingdom
[2]Escola Superior de Tecnologia e Gestão, Instituto Politécnico de Viana do Castelo, 4900–347 Viana do Castelo, Portugal
[3]Transport Phenomena Research Center, Faculty of Engineering, University of Porto, Rua Dr. Roberto Frais s/n, 4200–465 Porto, Portugal

[a]Author to whom correspondence should be addressed: michaelmc0993@gmail.com
[b]Electronic mail: T.A.E.Riou@leeds.ac.uk
[c]Electronic mail: pedroresende@estg.ipvc.pt
[d]Electronic mail: M.Wilson@leeds.ac.uk
[e]Electronic mail: aafonso@fe.up.pt
[f]Electronic mail: G.N.deBoer@leeds.ac.uk

ABSTRACT

A novel open-source anisotropic $k-\varepsilon-v^2-f$ model is presented for turbulent viscoelastic duct flow with dilute polymeric solutions described by the finitely extensible nonlinear elastic-Peterlin constitutive model. The turbulence model for channel and square duct flow of Newtonian fluids is adapted to incorporate the polymeric terms within the governing equations. All the required non-linear terms are validated with simple closure models and are assessed *a priori* against independent direct numerical simulation data in fully developed channel flow. The NLT_{ij} term, which accounts for the interaction between fluctuating components of the conformation tensor and the velocity gradient tensor, is modeled with the mean flow direction, t_i, and wall-normal, n_i, present in the Newtonian model, based on the streamwise alignment of mean polymer stretch. The implicit polymer effects on pressure–strain are assessed with a simple *ad hoc* closure accounting for the reduced near-wall production of turbulent kinetic energy. The same closure is also adapted for the spanwise Reynolds stress predictions of polymer-enhanced secondary flow. The model performs well in channel flow and captures low, intermediate, and high drag reduction features for a wide range of rheological parameters. The capabilities are extended for square ducts (or any regular polygon) due to the symmetric modeling of the closure models, which can predict the mean streamwise and secondary flow features associated with second normal Reynolds stress differences. Accessible codes and models are crucial for the advancement and improvement of turbulent viscoelastic models, and an OpenFOAM C++ code package is developed and freely available on GitHub (https://github.com/MikeMcDermott-Code/v2f).

NOMENCLATURE

C_{ij}	Mean conformation tensor
DNS	Direct numerical simulation
DR	Drag reduction
E^V	Newtonian destruction to the dissipation rate
f	Elliptic relaxation function
f_d	Newtonian spanwise distribution function
$f(C_{mm})$	Peterlin function
f_d^V	Viscoelastic spanwise distribution function
HDR	High drag reduction
h	Channel half height
IDR	Intermediate drag reduction
k	Turbulent kinetic energy
LDR	Low drag reduction
L_t	Turbulent length scale
L^2	Maximum extensibility of the dumbbell model
MDR	Maximum drag reduction
M_{ij}	Mean flow distortion term of the conformation tensor transport

NLT_{ij}	Non-linear term of the conformation tensor transport
N_{ij}	Redistribution term of Reynolds stress normal components
n_i	Wall normal direction
P	Mean kinematic pressure
P_h	"Wetted" perimeter
P_k	Mean rate of production of turbulent kinetic energy
RANS	Reynolds-averaged Navier–Stokes
RMS	Root mean square
RSM	Reynolds stress model
R_h	Hydraulic radius
Re_{τ_0}	Friction Reynolds number
S_{ij}	Mean rate of strain
T_t	Turbulent time scale
t_i	Mean vorticity direction
U_i	Mean velocity
u, v, w	Velocity components
v^2	Near wall Reynolds stress scaling
Wi_{τ_0}	Friction Weissenberg number
x, y, z	Streamwise, transverse, and spanwise directions

Greek symbols

γ	Shear rate magnitude
δ_{ij}	Kronecker delta
ε	Dissipation rate of turbulent kinetic energy
ε_{ijk}	Levi-Civita symbol
ε^V	Viscoelastic stress work of turbulent kinetic energy
$\varepsilon_{ijk}\kappa$	Artificial numerical diffusivity constant
λ	Relaxation time of polymeric fluid
ν_0	Total kinematic viscosity
ν_p	Polymer kinematic viscosity
ν_s	Solvent kinematic viscosity
ν_T	Kinematic eddy/turbulent viscosity
ρ	Fluid density
τ_{ij}	Shear stress tensor
ω_x	Mean stream-wise vorticity

Superscript/subscript

$\bar{a}, A$	Mean quantity
a_s	Newtonian/solvent quantity
a_w	Near wall quantity
a'	Fluctuating quantity
a^+	Normalized by friction velocity
a^V, a_p	Viscoelastic/polymeric quantity

I. INTRODUCTION

Numerical predictions of drag-reducing turbulent flows with polymer additives have gained much interest among engineers since the experimental finding of Toms.[1] Early studies in the literature quantify the behavior of turbulent polymer flows in channel and pipe flows.[2–4] The logarithmic velocity profile in polymer flow increases with respect to Newtonian flow, owing to a reduction in the near-wall turbulent fluctuations from the stretching of polymers, causing an effective thickening of the viscous sub-layer[2] and enhanced velocity profile, up to 80%, reaching a maximum drag reduction (MDR) limit.[5]

Over the last few decades, several experimental and direct numerical simulation (DNS) studies examined the energy exchanges between the polymer chains and turbulent structures, to investigate the mechanisms of drag-reducing channel flow,[6–10] with some notable reviews on these mechanisms.[11,12] For the numerical investigations, the finitely extensible nonlinear elastic-Peterlin (FENE-P) dumbbell model[13] has been predominantly used to represent the polymer chains, because of its molecular roots in kinetic theory. It is now known to at least low to moderate levels of drag reduction (DR) that the mechanism is the transfer of energy from the near-wall (buffer layer) streamwise vortices to polymers that stretch in the extensional flow and then relax as they are rolled into other vortices. This generates forces that tend to inhibit the hairpin vortices.[14] Quantitatively, this can be expressed as a polymer body force,[8] which is positive in the streamwise direction, with an opposite sign (anti-correlation) in the transverse and spanwise directions. These forces are also accompanied by a substantial reduction in the velocity–pressure gradients in the Reynolds stress transport,[6] leading to strong flow anisotropy. The two primary sources for vorticity production, the production from the mean velocity gradient and the mixed production, decrease drastically, in an almost symmetric fashion with increasing viscoelasticity.

There is a wealth of Reynolds-averaged DNS data[7–9,14–16] that examine the effects of the polymer chains in fully developed turbulent channel flow by varying the rheological and flow parameters, such as the viscosity ratio, β, friction Weissenberg number, Wi_τ, maximum chain extensibility of the dumbbell model, L^2, and friction Reynolds number, Re_τ. The data assist the development of viscoelastic turbulence models to predict flow features in channels and pipes for engineering applications. Although DNS studies in turbulent channel flow with FENE-P fluids are well documented, numerical simulations for other canonical systems are scarce, with some recent work for turbulent viscoelastic jets,[17] turbulent planar wakes,[18] turbulent flow with spherical particle suspensions,[19] and turbulent flow in square ducts.[20]

The enhanced streamwise features of turbulent polymer flows in square ducts are similar to those documented in channel flow, showing an increase in the mean velocity profile and thickening of the buffer layer, with a decrease in the wall-normal Reynolds stresses.[20] One of the key features of Newtonian turbulent flow in square ducts is the existence of secondary flow of the second kind,[21] predominantly generated from the production of Reynolds stress gradients.[22] The secondary flow in the cross-stream plane gives rise to bending of the mean streamwise velocity isolines toward the duct corners,[23] along with eight counter-rotating vortices.

Although the intensity of the secondary motion is small compared to the streamwise motion (usually a few percent), they are generally assumed to have some important practical impact in redistributing friction along the duct perimeter.[24] In the presence of polymers, the reduction in the wall-normal Reynolds stresses (or normal stress anisotropy) results in a shift of the maximum vorticity, moving toward the center of the duct.[20] The vorticity behavior is concurrent with the streamwise enstrophy budget in turbulent channel flows.[6] Further, recent work analyzing turbulent entrainment in viscoelastic jets suggest that regions of high enstrophy dynamics interact strongly with polymer stresses,[25] which shows good evidence that drag reduction and changes to the vorticity field are interconnected. Predicting secondary motion and vorticity features is of great interest for engineering purposes and toward a more general viscoelastic turbulence model for wall-bounded flows.

Many attempts have been made to predict the secondary flow features of Newtonian turbulent square duct flow in the context of Reynolds-averaged Navier–Stokes (RANS) modeling. It is well known that classical isotropic eddy viscosity models fail to capture the self-sustained secondary motion.[26] This necessitated the use of Non-Linear Eddy Viscosity Models,[27,28] in which the Boussinesq hypothesis is extended to have higher order dependence on the strain and vorticity rates, based on the polynomial tensor basis of Pope.[29] Pecnik and Iaccarino[30] developed the isotropic $k-\varepsilon-v^2-f$ model of Lien *et al.*[31] to predict normal stress anisotropy, and thus secondary flow features. The model obeys the linear eddy viscosity hypothesis, whilst introducing a non-isotropic contribution, N_{ij}, based on the wall Reynolds stress scalar, v^2, without relying on additional nonlinear terms. Modesti[32] performed *a priori* DNS tests on eddy viscosity models by quantifying their accuracy in predicting the wall-normal and shear Reynolds stress components in Newtonian turbulent square ducts. They concluded that the anisotropic v^2-f model performed best for both components, although it is not based on the nonlinear expansion.[29] Given that drag reduction in turbulent viscoelastic duct flow is associated with enhanced wall normal Reynolds stresses, the model of Pecnik and Iaccarino[30] is chosen for the Newtonian closures within this study. The $k-\epsilon-\phi-f$ of Laurence *et al.*[33] was considered as the baseline Newtonian model, where $\phi=v^2/k$. However, given that the $k-\epsilon-v^2-f$ model has shown promise for predicting Newtonian flow in square duct flows[30] and has also been applied for turbulent viscoelastic channel flows,[34] the $k-\epsilon-\phi-f$ model is beyond the scope of this work and will be considered within future implementations.

Leighton *et al.*[35] proposed the first turbulence model based on FENE-P fluids. The developed Reynolds stress model (RSM) laid the foundation of the governing equations, and the general nomenclature followed,[36] which is largely adapted by the proceeding literature. Pinho *et al.*[37] proposed a new RANS model which extended the Newtonian low-Reynolds number $k-\varepsilon$ model. Their work largely reduces the model complexity by analyzing the dominant contributions in the governing equations, to which closures were proposed and predictions up to Low Drag Reduction (LDR) were achieved. However, the turbulent kinetic energy exhibited a mean peak and global reduction, which opposed the experimental[7] and DNS findings.[38] Soon after, Resende *et al.*[39] extended the model capacity to the intermediate drag reduction (IDR) regime. This was achieved by improving the closure predictions for the nonlinear term of the conformation tensor equation (denoted NLT_{ij}), the viscoelastic stress work (denoted ε_{ij}^V), and the viscoelastic turbulent transport in the turbulent kinetic energy equation (denoted Q^V). The same model closures were adapted[40] to a $k-\omega$ Newtonian model, although the same limitations occur as previous[37,39] along with exceedingly complex model closures. Later, Resende *et al.*[41] improved the model capabilities to high drag reduction (HDR) regimes and reduced the complexity of the NLT_{ij} term, along with the correct increase for the turbulent kinetic energy via a modified damping function to include viscoelastic effects. This occurred by analyzing the change in the production term within the transport of k,[42] along with *a priori* DNS data analysis for a new NLT_{ij} relation.[43] The work was then extended to remove all friction velocity, bulk parameters, and reduce further the model complexity,[44] along with a $k-\omega$ counterpart, which includes β variation.[45] The model can predict all ranges of friction Reynolds numbers within the literature, along with a large range of rheological parameters. However, the model is limited to the isotropic context and does not feature the normal Reynolds stress anisotropy needed for secondary flow calculations, although the development of viscoelastic closures for the polymer stress tensor is important to this study.

Iaccarino *et al.*[46] proposed the first $k-\varepsilon-v^2-f$ model for FENE-P fluids in fully developed channel flow. The concept of a *turbulent polymer viscosity* was introduced, which accounts for the combined effect of turbulence with polymer chains on the polymer shear stress in the momentum equation. The turbulent polymer viscosity was modeled with direct dependence on the turbulent kinetic energy. The effect of the polymer chains on the rate of production was included implicitly, with a model for the viscoelastic stress work depending on the turbulent polymer viscosity. Masoudian *et al.*[15] later improved the closure model for the turbulent polymer viscosity with dependence on the local eddy viscosity. The viscoelastic stress work was modeled as it is within previous models,[37,39] along with an *ad hoc* model for the combined effects of the transverse viscoelastic stress work and pressure–strain term in the v^2 transport equation. The trace of NLT_{ij} is modeled with dependence on the local eddy viscosity and mean flow distortion term, which is shown to perform well for all ranges of DR. The model can predict all regimes of DR but contains friction velocity dependence which becomes problematic in flows with stagnation points. Masoudian *et al.*[34] extended the model capabilities to include heat transfer with a passive scalar temperature field. They also produce a Boussinesq-like closure for NLT_{ij}, which models both the polymer extension (NLT_{kk}), and the shear component (NLT_{xy}) that calculates the polymer shear stress in the momentum equation. However, this closure is misrepresented as the NLT_{xy} term has an opposite sign, as shown by the DNS.[47] Benzi[48] demonstrated in their toy model that the overall role of polymer stretching is to induce an effective polymer viscosity proportional to the transverse conformation tensor component, C_{yy}, which is dominated by the NLT_{yy} term (also see Fig. 1 in Pinho *et al.*[37] for further DNS). Masoudian *et al.*[49] produced a RSM which greatly improves flow predictions from Leighton *et al.*[35] The NLT_{ij} closure is made proportional to the Reynolds stress tensor by analyzing the events of the two fields, although requiring an additional damping function to correct the near-wall behavior.

In general, the availability of developed open-source code packages is desirable for advancing research. Many works, with respect to RANS turbulent viscoelastic flow modeling, operate with in-house codes with FORTRAN.[15,34,37,39,50] Commercial software, Ansys, has been adapted to include the $k-\varepsilon-v^2-f$ model[15] with user-defined functions,[51] along with OpenFOAM[52] for the same model,[15] although the code is not readily available. A good modern review of numerical methods and challenges for turbulent viscoelastic flows including the FENE-P model can be viewed in the work of Alves *et al.*[53]

In the present study, the anisotropic $k-\varepsilon-v^2-f$ model for Newtonian fluids[30] is adapted to predict polymer flow features in fully developed turbulent channel flows, and more generally, regular polygons such as square ducts. The model capabilities could extend to other wall-bounded flows such as a turbulent diffuser, but is here untested and beyond the scope of this work. The NLT_{ij} term modeling within previous studies is assessed and adapted for wall-bounded flows. The overall model is validated and assessed against independent DNS data in turbulent viscoelastic channel flow for LDR, IDR, and

HDR. The NLT_{ij} model coefficients are adapted and applied to square duct flow data[20] at IDR. An OpenFOAM C++ code is developed by creating a base class for the $k-\varepsilon-v^2-f$ model based on Newtonian fluids,[30] then adapted to incorporate the conformation transport equations and properties. The source code, case folders, and accompanying configuration files are freely available here (https://github.com/MikeMcDermott-Code/v2f). The paper is organized as follows: Sec. II introduces the Reynolds-averaged governing equations appropriate for wall-bounded turbulent polymer flow; Sec. III explains in detail the development of viscoelastic turbulent closures; Sec. IV summarizes the present model; Sec. V presents the numerical procedure and accompanying studies; Sec. VI presents the results; and finally in Sec. VII, the main conclusions are presented.

II. GOVERNING EQUATIONS

The governing equations appropriate for fully developed, steady state, incompressible turbulent flow of dilute polymer solutions are presented in Subsections II A–II D. Overbars or upper-case represent Reynolds-averaged quantities, and primes or lower-case represent the fluctuating quantities. For brevity, the computational domain for fully developed channel flow and square duct flow can be viewed in Fig. 1, which represent one-half and one-quarter of the full domain, respectively, with channel half-height, h, defined. The direction of the mean flow, t_x, and wall-normal, n_i, is described mathematically in the proceeding sections.

A. Continuity and momentum equations

The Reynolds-averaged continuity and momentum equations are, respectively,

$$\frac{\partial U_i}{\partial x_i} = 0, \tag{1}$$

$$U_j \frac{\partial U_i}{\partial x_j} = -\frac{\partial P}{\partial x_i} + \frac{\partial}{\partial x_j}\left(\bar{\tau}_{ij} - \overline{u_i' u_j'}\right), \tag{2}$$

where U_i is the mean velocity, P is the mean kinematic pressure, $\bar{\tau}_{ij}$ is the mean extra stress tensor, and $\overline{u_i' u_j'}$ is the Reynolds stress tensor. $\bar{\tau}_{ij}$ describes the rheology of the fluid and is given in Eq. (3) as the sum of a Newtonian solvent contribution of kinematic viscosity, ν_s, with a polymeric contribution $\bar{\tau}_{ij,p}$ described by the FENE-P rheological constitutive model,[13]

$$\bar{\tau}_{ij} = \nu_s S_{ij} + \bar{\tau}_{ij,p}, \tag{3}$$

where S_{ij} is the mean strain rate tensor defined by

$$S_{ij} = \frac{1}{2}\left(\frac{\partial U_i}{\partial x_j} + \frac{\partial U_j}{\partial x_i}\right). \tag{4}$$

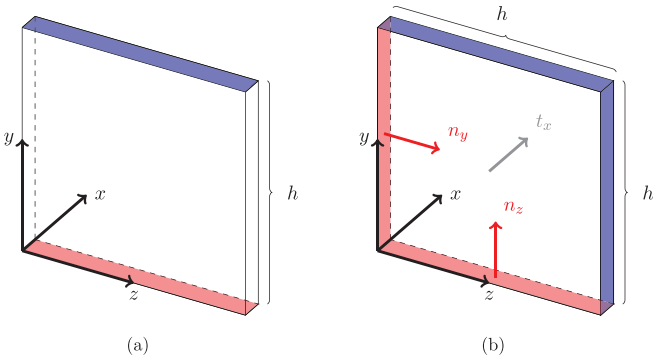

FIG. 1. Computational domain for (a) channel flow and (b) square duct flow, with channel half-height, h. The direction of the mean flow, t_x, coincides with the streamwise direction, with wall normals, n_i, displayed. The red and blue patches are the wall and symmetry planes, respectively.

B. Constitutive equation

The Reynolds-averaged equation of the polymeric stress for a FENE-P dumbbell model is well documented[37] and is represented by an explicit function of the mean conformation tensor, C_{ij}, given by

$$\bar{\tau}_{ij,p} = \frac{\nu_p}{\lambda}\left[\overline{f(C_{kk}+c_{kk}')(C_{ij}+c_{ij}')} - f(L)\delta_{ij}\right], \tag{5}$$

$$f(C_{mm}) = \frac{L^2-3}{L^2-C_{kk}} \quad \text{and} \quad f(L) = 1, \tag{6}$$

where ν_p is the kinematic polymeric viscosity, λ is the relaxation time, and L^2 denotes the maximum molecular extensibility of the model dumbbell.

The behavior of the mean conformation tensor, C_{ij}, follows a hyperbolic differential equation known as the Reynolds-averaged conformation evolution (RACE), of the form

$$U_k \frac{\partial C_{ij}}{\partial x_k} - M_{ij} - CT_{ij} - NLT_{ij} = -\frac{\bar{\tau}_{ij,p}}{\nu_p}, \tag{7}$$

$$M_{ij} = C_{jk}\frac{\partial U_i}{\partial x_k} + C_{ik}\frac{\partial U_j}{\partial x_k}, \tag{8}$$

$$CT_{ij} = \overline{u_k' \frac{\partial c_{ij}'}{\partial x_k}}, \tag{9}$$

$$NLT_{ij} = \overline{c_{jk}' \frac{\partial u_i'}{\partial x_k}} + \overline{c_{ik}' \frac{\partial u_j'}{\partial x_k}}. \tag{10}$$

Here, M_{ij} is the mean flow distortion term; it is non-zero, but requires no closure. The remaining two terms are named following the nomenclature of Li *et al.*[38] and Housiadas *et al.*[54] They are labeled with CT_{ij}, representing the contribution to the transport of the conformation tensor due to the fluctuating advective terms, and NLT_{ij}, which accounts for the interactions between the fluctuating components of the conformation tensor and the velocity gradient tensor.

C. Reynolds stresses

The Reynolds stress tensor is computed with the model of Pecnik and Iaccarino,[30] which adopts a "linear" (the linearity holds because $\overline{u_m' u_m'} = 2k$, however, non-isotropic) Boussinesq turbulent stress–strain relationship,

$$-\overline{u_i' u_j'} \approx 2\nu_t S_{ij} - \left(\frac{2}{3}\delta_{ij} + N_{ij}\right)k, \tag{11}$$

where ν_t is the eddy viscosity, k is the turbulent kinetic energy, and N_{ij} is formulated to redistribute k in the normal components such that the trace of N_{ij} has to preserve $N_{ij}\delta_{ij} = 0$. The full derivation can be found in Pecnik and Iaccarino[30] and is here represented by

$$N_{ij} = \left(1 - \frac{3}{2}\frac{v^2}{k}\right)\left(\frac{\delta_{ij}}{3} - n_i n_j\right) + \left(\frac{2 - f_d}{2 + f_d} - \frac{1}{2}\frac{v^2}{k}\right)(2t_i t_j + n_i n_j - \delta_{ij}). \quad (12)$$

The first term within Eq. (12) ensures that the wall-normal fluctuating Reynolds stress $\overline{v'^2} = v^2$ and fulfills the physical requirements, which are zero trace and vanishing contribution in isotropic flow regions where $v^2 = \frac{2}{3}k$. The wall-normal is represented by a normalized gradient of a general variable ϕ,

$$n_i = \frac{\partial \phi}{\partial x_i} \Big/ \sqrt{\frac{\partial \phi}{\partial x_j}\frac{\partial \phi}{\partial x_j}}, \quad (13)$$

such that ϕ solves an elliptic relaxation equation given as

$$\frac{\partial^2 \phi}{\partial x_k \partial x_k} = -1, \quad (14)$$

typically used to obtain smooth variations of the wall distance in complex geometries.[55] At solid walls, $\phi = 0$, and $\partial\phi/\partial x_i = 0$ at open boundaries.

The second term in Eq. (12) removes the equality of $\overline{u'^2} = \overline{w'^2} = k - \frac{1}{2}v^2$, which would be the case for Eq. (12) containing just the first term. The function f_d is represented as

$$f_d = \min\left[\max\left(\left(\frac{3}{2}\frac{v^2}{k}\right)^{1/2}, 0.3\right), 1.0\right]. \quad (15)$$

This function ensures the correct asymptotic behavior of the components parallel to the wall so that $\overline{u'^2} \propto y^2$ and $\overline{w'^2} \propto y^2$. This was achieved by setting the damping function to a constant value of $f_{d0} = 0.3$ until $y^+ \approx 10$ given the DNS data.[56] Above this y^+ value, the damping function is modeled as a function of v^2/k.

The normalized direction of the largest normal Reynolds stress component, t_i, is assumed to coincide with the normalized velocity gradient.[30] This is a reasonable assumption for our studies in pressure-driven wall-bounded flows. More generally, t_i can coincide with the mean direction of vorticity such that

$$t_i \sim \frac{\omega_i}{|\omega_i|} = \epsilon_{ijk}\frac{\partial U_j}{\partial x_k} \Big/ \gamma, \quad (16)$$

where ϵ_{ijk} is the Levi-Civita symbol, ω_i is the vorticity, and $\gamma = \sqrt{S_{ij}S_{ij}}$ is the shear rate magnitude.

In this work, the eddy viscosity is modeled by the $k - \varepsilon - v^2 - f$ formulation of Lien *et al.*[31] This particular choice of model is justified by the fact that the polymer drag reduction is mostly a near wall phenomenon, and it requires a modification to the turbulence redistribution mechanism. The model represents a comprehensive and accurate approach to capture these aspects of turbulent boundary layers within a Boussinesq framework. The near-wall eddy viscosity model is inspired by the physics of the full Reynolds stress transport model, but retains only the wall-normal Reynolds stress scalar, $\overline{v^2}$, and its source, kf, representing the redistribution by pressure fluctuations. Then, in the classical closure for the eddy viscosity ($\nu_t \propto \frac{k^2}{\varepsilon}$) the wall damping effect is obtained by substituting one instance of k by v^2 as

$$\nu_t = C_\mu v^2 T_t, \quad (17)$$

where C_μ is a constant coefficient, v^2 is the transverse (wall-normal) Reynolds stress scalar, and T_t is the turbulent timescale defined as

$$T_t = \max\left\{\frac{k}{\varepsilon}, C_T\sqrt{\frac{\nu_0}{\varepsilon}}\right\}, \quad (18)$$

where $\nu_0 = \nu_s + \nu_p$ is the total viscosity, ε is the Newtonian rate of dissipation of k, and C_T is a constant coefficient.

The turbulence model for Newtonian fluids has three transport equations for k, ε, v^2, and one elliptic equation for f, and it accurately reproduces the parabolic decay of $v^2 = k$ down to the solid wall without introducing the wall-distance or low-Reynolds number damping functions in the eddy viscosity and $k - \varepsilon$ equations, which would then need to be modified to account for viscoelastic fluids.

The governing transport equation for the turbulent kinetic energy, k, with FENE-P fluids is given by[15]

$$U_j\frac{\partial k}{\partial x_j} = \frac{\partial}{\partial x_j}\left[\left(\nu_s + \frac{\nu_t}{\sigma_k}\right)\frac{\partial k}{\partial x_j}\right] + P_k - \varepsilon + Q^V - \varepsilon^V, \quad (19)$$

where $P_k = \overline{u_i' u_j'} S_{ij}$ is the mean rate of production of k, and σ_k is a constant coefficient. The last two terms on the right side of Eq. (19) are

$$Q^V = \frac{\partial \overline{\tau_{ik,p}' u_i'}}{\partial x_k} \quad \text{and} \quad \varepsilon^V = \overline{\tau_{ik,p}'\frac{\partial u_i'}{\partial x_k}}, \quad (20)$$

which are the viscoelastic turbulent transport and the viscoelastic stress work, respectively. They represent the fluctuating viscoelastic turbulent part of the k transport equation and require suitable closure models.

The corresponding governing transport equation for ε is given by

$$U_j\frac{\partial \varepsilon}{\partial x_j} = \frac{\partial}{\partial x_j}\left[\left(\nu_s + \frac{\nu_t}{\sigma_\varepsilon}\right)\frac{\partial \varepsilon}{\partial x_j}\right] + \frac{C_{\varepsilon 1}P_k - C_{\varepsilon 2}\varepsilon}{T_t} - E^V, \quad (21)$$

where σ_ε, $C_{\varepsilon 1}$, and $C_{\varepsilon 2}$ are the constant coefficients. The last term on the right side of Eq. (21) is the viscoelastic contribution to the overall ε balance,

$$E^V = 2\nu_s\overline{\frac{\partial u_i'}{\partial x_k}\frac{\partial}{\partial x_k}\left(\frac{\partial \tau_{ij,p}'}{\partial x_j}\right)}, \quad (22)$$

which has non-negligible effects on flow predictions for all DR regimes and thus requires a suitable closure model.

The transport equation for the scalar wall Reynolds stress, v^2, is given by

$$U_j\frac{\partial v^2}{\partial x_j} = \frac{\partial}{\partial x_j}\left[\left(\nu_s + \frac{\nu_t}{\sigma_k}\right)\frac{\partial v^2}{\partial x_j}\right] + kf - 6\frac{\varepsilon}{k}v^2 + Q^V_{v^2} - \varepsilon^V_{v^2}, \quad (23)$$

where f is the turbulence energy redistribution, and the last two terms on the right side are the analogous transverse components of Eq. (20), which require suitable closure models.

The corresponding governing transport equation for f is derived from the pressure–strain correlation[57,58] in the full Reynolds stress transport equation, given by

$$f - L_t^2 \frac{\partial^2 f}{\partial x_j \partial x_j} = \frac{1}{T_t}\left(\frac{2}{3}(C_1 - 1) - (C_1 - 6)\frac{v^2}{k}\right) + C_2 \frac{P_k}{k}, \quad (24)$$

with the length scale defined as

$$L_t^2 = C_L^2 \max\left\{\frac{k^3}{\varepsilon^2}, C_\eta^2\sqrt{\frac{\nu_0^3}{\varepsilon}}\right\}, \quad (25)$$

where C_1, C_2, C_L, and C_η are the constant coefficients.

D. Streamwise vorticity equation

The origins of mean secondary flow in fully developed turbulent polymer duct flow are found within the mean streamwise vorticity, ω_x, transport equation (see the Appendix within Ref. 20)

$$\frac{\partial \bar{\omega}_x}{\partial t} = \underbrace{\bar{v}\frac{\partial \bar{\omega}_x}{\partial y} + \bar{w}\frac{\partial \bar{\omega}_x}{\partial z}}_{\mathcal{C}} + \underbrace{\frac{\partial^2}{\partial y \partial z}\left(\overline{w'w'} - \overline{v'v'}\right)}_{\mathcal{A}} + \underbrace{\left(\frac{\partial^2}{\partial y^2} - \frac{\partial^2}{\partial z^2}\right)\overline{v'w'}}_{\mathcal{D}} - \underbrace{\frac{\beta}{Re}\left(\frac{\partial^2}{\partial y^2} + \frac{\partial^2}{\partial z^2}\right)\bar{\omega}_x}_{\mathcal{V}} - \underbrace{\frac{1-\beta}{Re}\left(\frac{\partial^2 \bar{\tau}_{yz,\mathrm{p}}}{\partial y^2} + \frac{\partial^2 \bar{\tau}_{zz,\mathrm{p}}}{\partial y \partial z} - \frac{\partial^2 \bar{\tau}_{yy,\mathrm{p}}}{\partial y \partial z} - \frac{\partial^2 \bar{\tau}_{yz,\mathrm{p}}}{\partial z^2}\right)}_{\mathcal{P}}, \quad (26)$$

where $\mathcal{C}$ is the convection of the mean vorticity by the secondary motion; $\mathcal{A}$ is the production term associated with the anisotropy of the in-plane normal stresses; $\mathcal{D}$ is the production/dissipation term due to the cross-stream Reynolds stress component, $\overline{v'w'}$; $\mathcal{V}$ is the viscous dissipation; and $\mathcal{P}$ is the polymeric contribution.

The budget analysis of Eq. (26) in polymeric square duct flow was performed by Shahmardi *et al.*[20] (Fig. 13 in their work). The dominant contributions in both Newtonian and polymeric flows are from $\mathcal{A}$ and $\mathcal{V}$. Although D is non-zero, it is over 10 times smaller in magnitude than A. Thus, it will be neglected in this study. The convection term, C, along with P are negligible. It is interesting to note that although the polymeric contribution to $\overline{\omega_x}$ is small in amplitude, the presence of the polymer produces macroscopic changes to the flow, by reducing the anisotropy of the in-plane velocity fluctuations.

III. DEVELOPMENT OF VISCOELASTIC CLOSURES

In this section, the non-linear viscoelastic terms requiring closures identified in Sec. II are developed *a priori* with gathered independent DNS data in turbulent viscoelastic channel and square duct flow for cases 7, 10, and 11 as described in Table I. The data availability for the NLT_{ij} term is exclusively from cases 7, 10, and 11 ($Re_{\tau_0} = 395$, $Wi_{\tau_0} = 25$ and 100, $L^2 = 900$ and 3600), which pertains to intermediate friction Reynolds number spanning low to high DR, which is used to validate the current model closures. This selected data are also assessed within multiple studies of RANS FENE-P modeling.[15,34,41,44,45,49] A broad range of rheological parameters ($Re_{\tau_0} = 180$–1000, $\beta = 0.9$, $Wi_{\tau_0} = 18$–100, $L^2 = 900$–3600) are selected with low to high DR for channel flow and intermediate DR for square ducts to test the model performance on predicting mean field values such as velocity, Reynolds stresses, conformation tensor, and secondary flow, within the results section. All future mentions of "Case x" are referred to by Table I.

TABLE I. Independent DNS data of fully developed turbulent channel and square duct flow for FENE-P fluids with DR model predictions.

		Rheological parameters				DR (%)	
Case	References	$Re_{\tau_0} = \frac{hu_\tau}{\nu_0}$	$\beta = \frac{\nu_s}{\nu_0}$	$Wi_{\tau_0} = \frac{\lambda u_\tau^2}{\nu_0}$	L^2	DNS	Model
Channel:							
(1)	Masoudian *et al.*[15]	180	0.9	25	900	19	25
(2)	Li *et al.*[9]	180	0.9	50	900	31	30
(3)	Masoudian *et al.*[15]	180	0.9	100	900	38	37
(4)	Masoudian *et al.*[15]	180	0.9	100	3600	54	46
(5)	Iaccarino *et al.*[46]	300	0.9	36	3600	33	27
(6)	Iaccarino *et al.*[46]	300	0.9	60	3600	47	36
(7)	Masoudian *et al.*[34]	395	0.9	25	900	19	23
(8)	Masoudian *et al.*[34]	395	0.9	50	900	30	27
(9)	Masoudian *et al.*[34]	395	0.9	50	3600	38	31
(10)	Masoudian *et al.*[34]	395	0.9	100	900	37	35
(11)	Masoudian *et al.*[34]	395	0.9	100	3600	48	46
(12)	Masoudian *et al.*[34]	590	0.9	50	3600	39	29
(13)	Thais *et al.*[10]	1000	0.9	50	900	30	26
Square duct:							
(A)	Shahmardi *et al.*[20]	366	0.9	18	900	25	25
(B)	Shahmardi *et al.*[20]	366	0.9	36	900	29	29

A. Closures for the conformation tensor

The first term that needs a closure is the mean polymer stress, Eq. (5). The expansion of this term can be written in the form

$$\bar{\tau}_{ij,\mathrm{p}} = \frac{\nu_\mathrm{p}}{\lambda}\left[f(C_{kk})C_{ij} - f(L)\delta_{ij}\right] + \frac{\nu_\mathrm{p}}{\lambda}\left[\overline{f(C_{kk}+c'_{kk})(C_{ij}+c'_{ij})} - f(C_{kk})C_{ij}\right]. \quad (27)$$

The magnitude of both terms on the RHS of Eq. (27) was analyzed *a priori* using DNS data.[37] This analysis showed that at different values of L^2 and Wi_{τ_0}, the first term is nearly 20 times larger regardless of the rheological parameters. In this study, the mean polymer stress is approximated by the first term as with other models,[15,34,40,46] hence given by

$$\bar{\tau}_{ij,\mathrm{p}} = \frac{\nu_\mathrm{p}}{\lambda}\left[f(C_{kk})C_{ij} - f(L)\delta_{ij}\right]. \quad (28)$$

The CT_{ij} term can be omitted for all DR regimes following a budget analysis of Eq. (7) carried out by Housiadas *et al.*[54] and Li *et al.*[38] The NLT_{ij} term cannot be neglected since it is a significant contributor in Eq. (7) and therefore requires a suitable closure.

To compute the polymer stress, one must calculate the components of the mean conformation tensor, C_{ij}, via the RACE [Eq. (7)]. The set of analytical equations for fully developed channel flow can be viewed in Appendix 1 of Ref. 37. In square ducts, there are walls in the y and z directions, such that

$$\begin{aligned}\bar{\tau}_{xy,\mathrm{p}} + \bar{\tau}_{xz,\mathrm{p}} &= \frac{\nu_\mathrm{p}}{\lambda} f(C_{kk})(C_{xy}+C_{xz}) \\ &= \nu_\mathrm{p}(NLT_{xy}+NLT_{xz}) \\ &\quad + \frac{\nu_\mathrm{p}}{f(C_{mm})}\left(\left(\lambda NLT_{yy}+1\right)\frac{\mathrm{d}U}{\mathrm{d}y} + \left(\lambda NLT_{zz}+1\right)\frac{\mathrm{d}U}{\mathrm{d}z}\right).\end{aligned} \quad (29)$$

For channel flow, the xz and zz terms are zero, and the transverse component is strictly in yy. For square duct flow, with symmetry along $y = z$, the terms in $\bar{\tau}_{xy,\mathrm{p}}$ and $\bar{\tau}_{xz,\mathrm{p}}$ are identical. Going forward, without loss of generality, xy, and yy are referred to as the shear and transverse components, respectively— with the zz term denoted as spanwise.

The NLT_{ij} components (xx, yy, zz, and xy) require careful consideration for accurate predictions of the polymer shear stress. It was demonstrated by Masoudian *et al.*[49] that NLT_{ij} and $\overline{u'_i u'_j}$ have a similarity of events, based on their iso-surface projections. This can be approximated with the assumption for the NLT_{ij} normal components as follows:

$$NLT_{ij} \sim \frac{\overline{u'_i u'_j}}{2k} NLT_{kk}. \quad (30)$$

Figure 2 displays *a priori* DNS results of Eq. (30) for case 7. The correlations show a similar behavior with the DNS data, capturing peak locations and trends well with the Reynolds stress tensor distributing NLT_{kk}. Benzi[48] characterizes an ordering of each C_{ij} term based on scale analysis such that $C_{xx} \sim 1/\Delta$, $C_{xy} \sim O(1)$, and $C_{yy} = C_{zz} \sim \Delta$, where Δ is some small number. This is also reflected for the corresponding NLT_{ij} terms.

Instead of considering the full Reynolds normal stress approximation in Eq. (30), a more simplistic approach is taken. The stretching

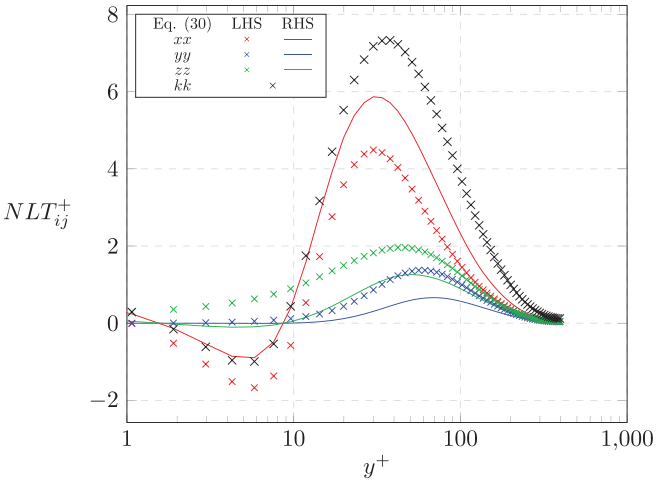

FIG. 2. *A priori* analysis of NLT^+_{ij} [Eq. (30)] in fully developed channel flow with DNS data case 7.

of the polymer chains is accounted for by NLT_{kk}, which is dominated by the streamwise component, as the chains tend to align with the mean streamwise vortices or enstrophy,[6] here represented by t_i from the Newtonian model [Eq. (16)], such that

$$NLT_{xx} = NLT_{ij}t_i t_j \sim NLT_{kk}. \quad (31)$$

A closure model is required for the scalar quantity, NLT_{kk}, which is here given by the Masoudian *et al.*[15] model, $NLT_{kk} = C_{V1}(\nu_\mathrm{t}/\nu_0)M_{kk}$, where C_{V1} is a constant coefficient. Present within the DNS data is the occurrence of a small near-wall negative peak. According to Dubief *et al.*[59] and Leighton *et al.*,[35] this has some impact on the near wall energy transfer from the polymers to the turbulence (opposite to the global energy transfer), although there is no mention within the literature of a mechanistic role. This term could cause numerical instability due to the rapid changes in the buffer layer and was neglected by Masoudian *et al.*,[15,34] and is also the case here.

Benzi[48] demonstrated in their toy model that the overall role of polymer stretching is to induce an effective polymer viscosity proportional to the transverse conformation tensor component, C_{yy}, which is determined by NLT_{yy}. This relationship is represented as

$$NLT_{yy} = NLT_{v^2} \sim \frac{v^2}{k} NLT_{kk}. \quad (32)$$

Figure 3 displays *a priori* DNS results of Eq. (32) for cases 7, 10, and 11. The trend holds well for all levels of DR, especially capturing the peak locations and shift away from the buffer layer. The NLT_{zz} component was shown by Pinho *et al.*[37] to have a small impact on overall model predictions in fully developed channel flow. This is due to the fact that the presence of NLT_{zz} in the model equations is only via the NLT_{kk} term, which is dominated by NLT_{xx}, and is therefore neglected.

The NLT_{xy} component has been previously modeled directly via dependence on M_{ij},[44,45] which also captured the small negative peak in NLT_{xx} in their modeling. Masoudian *et al.*[34] developed a Bousinesq-like closure for NLT_{ij}, which was made proportional to M_{ij}, meaning the polymer shear stress was proportional to NLT_{xy}. However, with this approach, NLT_{yy} is defined to be zero, and NLT_{xy} is defined to be

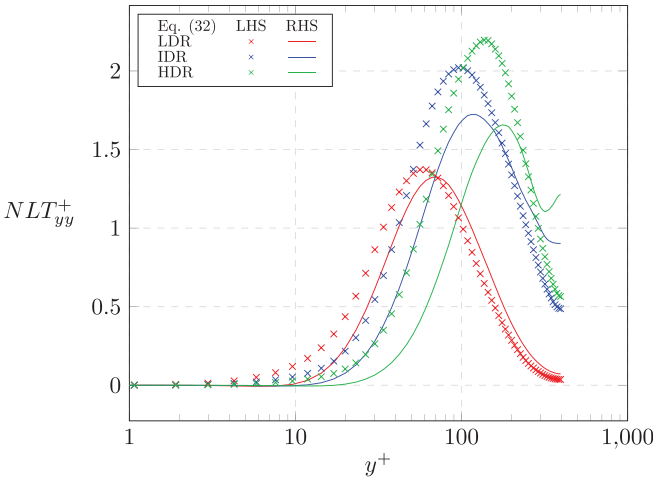

FIG. 3. *A priori* analysis of NLT^+_{yy} [Eq. (32)] in fully developed channel flow with DNS data for LDR (case 7), IDR (case 10), and HDR (case 11).

positive which is contradictory to the DNS findings. The NLT_{xy} term has less impact near the wall and buffer layer for polymer shear stress predictions from DNS data studies[37] and is thus neglected. The overall model for NLT_{ij} is presented as

$$NLT_{ij} = C_{V1}\frac{\nu_t}{\nu_0}M_{kk}\left(t_i t_j + C_{V2}\frac{v^2}{k}n_i n_j\right), \tag{33}$$

where C_{V2} is a model coefficient. Note that the key feature in Eq. (33) is adopting the simple and effective closure model for the scalar quantity $NLT_{kk} = C_{V1}(\nu_t/\nu_0)M_{kk}$, with redistribution in the dominant streamwise direction, and in the transverse direction with the natural scaling v^2/k. The effect of NLT_{ij} on the mean conformation tensor, C_{ij}, is analyzed in the results section against DNS data for both channel flow and square duct flow.

B. Closures for the transport of k, ε, v^2, and f

Budget analysis for each term in the k transport equation was performed by Pinho *et al.*[37] for different regimes of DR. They demonstrated that the magnitude of Q^V has more impact on the overall budget in the IDR regime and also developed a closure. In the HDR regime, the amplitude of Q^V is the same as ε^V but has a different location in the buffer layer, in which the effects of Q^V are overcome by turbulent diffusion, thus revealing negligible effects to overall flow predictions. Previous models[15,34,41,44,45] chose to neglect the Q^V contributions, and it is also not included here as well.

The closure model for the viscoelastic stress work is well founded[37,44,49] and is presented as

$$\varepsilon^V_{ij} = \frac{\nu_p}{2\lambda}f(C_{mm})NLT_{ij}. \tag{34}$$

Masoudian *et al.*[15] confirmed the model capabilities within 5% accuracy for all DR regimes via a probability density function study. The viscoelastic closure in the k transport is

$$\varepsilon^V_{kk} \equiv \varepsilon^V = \frac{\nu_p}{2\lambda}f(C_{mm})NLT_{kk}. \tag{35}$$

The viscoelastic contribution to the dissipation transport equation, E^V, is modeled in the same manner as previous models,[15,34,39] with a ratio of the viscoelastic stress work and turbulent timescale

$$E^V = \frac{C_{\varepsilon 1}\varepsilon^V}{T_t}. \tag{36}$$

The transverse viscoelastic stress work, $\varepsilon^V_{v^2}$, in the transport of v^2 can be simply deduced from the current model for NLT_{ij}, viz.,

$$\varepsilon^V_{v^2} = C_{V2}\frac{v^2}{k}\varepsilon^V, \tag{37}$$

so that the transport equation of v^2 can be recast as

$$U_j\frac{\partial v^2}{\partial x_j} = \frac{\partial}{\partial x_j}\left[\left(\nu_s + \frac{\nu_t}{\sigma_k}\right)\frac{\partial v^2}{\partial x_j}\right] + kf - \left(6\varepsilon + C_{V2}\varepsilon^V\right)\frac{v^2}{k}. \tag{38}$$

The production term above, kf, reduces monotonically for increasing DR. Given that k increases with DR, there must be a substantial reduction in the redistribution term, f. Modifications of the fluctuating pressure field represent implicit polymer effects which limit pressure–strain redistribution and hence the production of turbulent shear stress. Limited closure models are available for the viscoelastic contributions to pressure–strain in turbulent viscoelastic flows. Leighton *et al.*[35] first produced a closure proportional to the rapid pressure–strain term [first term on RHS of Eq. (24)], with some viscoelastic quantities. In their RSM, the closure required an additional damping function and was later found to completely relaminarize the flow at HDR.[46] Iaccarino[46] proposed a modification to the production term to account for the implicit effects of the polymer chains, with an effective rate of production, $P_k - \varepsilon^V$, where ε^V represents the energy transfer via polymer stretching. The closures developed in the model were shown to perform poorly, with excessive damping in the log-layer.[15] Masoudian *et al.*[15,34] modeled v^2 *ad hoc* by recasting the production term, kf, to include viscoelastic effects via $kf(1-g)$, where g are some viscoelastic quantities. The difficulty with this closure is for when $g > 1$ in any part of the flow domain, the pressure term becomes negative and causes complete flow relaminarization or code instability, as remarked in Refs. 34 and 52. Later, slight improvements are made to the closure parameters,[34] although the same functional form is maintained.

Here, a simple *ad hoc* closure is proposed, which recasts the production term constant, $C_2 \to \frac{C_2}{1+C_{V3}f(C_{kk})\sqrt{L^2}}$, where C_{V3} is a constant coefficient. Figure 4 displays *a priori* DNS results for the function $\frac{1}{1+f(C_{kk})\sqrt{L^2}}$ for cases 7, 10, and 11. There is a reasonable proportionality with DR which ensures the reduction of turbulent production via implicit near wall polymer effects, leading to Reynolds streamwise stress increase and anisotropy. The predictions on the Reynolds normal stresses are highlighted in the results section. The transport equation of f is recast as

$$f - L_t^2\frac{\partial^2 f}{\partial x_j \partial x_j} = \frac{1}{T_t}\left(\frac{2}{3}(C_1 - 1) - (C_1 - 6)\frac{v^2}{k}\right) + \frac{C_2}{1 + C_{V3}f(C_{kk})\sqrt{L^2}}\frac{P_k}{k}. \tag{39}$$

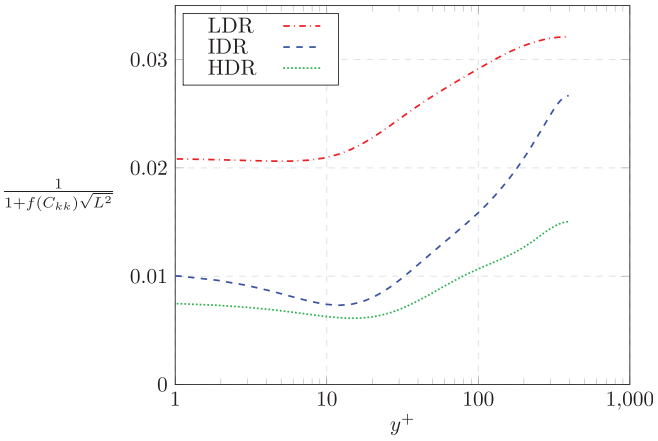

FIG. 4. *A priori* analysis of the *ad hoc* function $\frac{1}{1+f(C_{kk})\sqrt{L^2}}$ in fully developed channel flow with DNS data for LDR (case 7), IDR (case 10), and HDR (case 11).

C. Closure for span-wise Reynolds stress

The $\overline{w'^2}$ term requires a closure model for viscoelastic effects as predictions are important in the production of streamwise vorticity. The functional form of the Newtonian model[30] is given by

$$\overline{w'^2} = \frac{f_d}{2}\left(\overline{u'^2} + \overline{v'^2}\right), \tag{40}$$

and

$$f_d = \min\left[\max\left(\left(\frac{3}{2}\frac{v^2}{k}\right)^{1/2}, 0.3\right), 1.0\right]. \tag{41}$$

The damping function, f_d, was introduced to ensure the correct asymptotic behavior of the components parallel to the wall so that $\overline{u'^2} \propto y^2$ and $\overline{w'^2} \propto y^2$. This was achieved by setting the damping function to a constant value of $f_{d0} = 0.3$ until $y^+ \approx 10$ given the DNS data.[56] Above this y^+ value, the damping function is modeled as a function of v^2/k. For turbulent viscoelastic flow, $\overline{w'^2}$ reduces in the near wall for increasing DR, in a similar fashion to $\overline{v'^2}$. This near-wall reduction is approximated with the same *ad hoc* closure derived in Subsection III B, viz.,

$$f_d^V = \min\left[\max\left(\left(\frac{3}{2}\frac{v^2}{k}\right)^{1/2}, \frac{0.3}{1 + C_{V3} f(C_{kk})\sqrt{L^2}}\right), 1.0\right]. \tag{42}$$

Figure 5 displays *a priori* analysis of $\overline{w'^2}$ [Eq. (40)] in fully developed channel flow with DNS data of Newtonian[56] and case 7. General trends are captured well, with the near-wall reduction through the *ad hoc* closure, along with the overall reduction away from the v^2 component.

IV. SUMMARY OF THE PRESENT MODEL

The governing equations with complete closure models that were developed in Secs. III are summarized below:

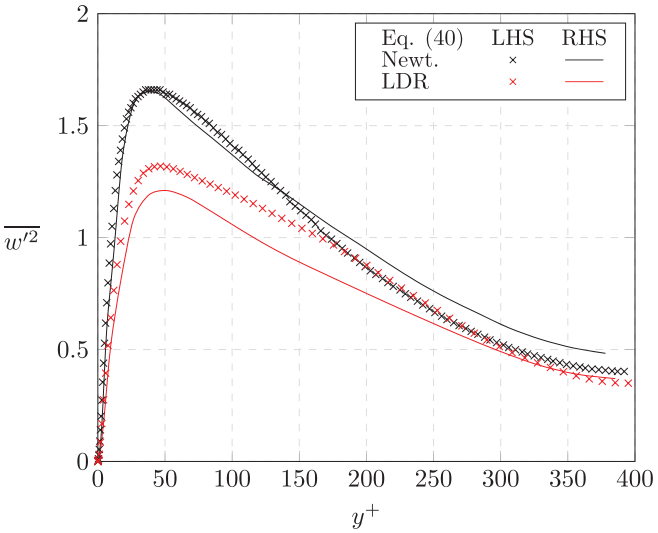

FIG. 5. *A priori* analysis of $\overline{w'^2}$ [Eq. (40)] in fully developed channel flow with DNS data of Newtonian and case 7.

Continuity equation

$$\frac{\partial U_i}{\partial x_i} = 0. \tag{43}$$

Momentum transport equation

$$U_j\frac{\partial U_i}{\partial x_j} = -\frac{\partial P}{\partial x_i} + \frac{\partial}{\partial x_j}\left((\nu_s + \nu_t)\frac{\partial U_i}{\partial x_j} - \left(\frac{2}{3}\delta_{ij} + N_{ij}\right)k + \frac{\nu_p}{\lambda}\left(f(C_{kk})C_{ij} - \delta_{ij}\right)\right), \tag{44}$$

where the eddy viscosity is

$$\nu_t = C_\mu v^2 T_t, \tag{45}$$

and the normal Reynolds stress distribution term is

$$N_{ij} = \left(1 - \frac{3}{2}\frac{v^2}{k}\right)\left(\frac{\delta_{ij}}{3} - n_i n_j\right) + \left(\frac{2 - f_d^V}{2 + f_d^V} - \frac{1}{2}\frac{v^2}{k}\right)(2t_i t_j + n_i n_j - \delta_{ij}), \tag{46}$$

with

$$f_d^V = \min\left[\max\left(\left(\frac{3}{2}\frac{v^2}{k}\right)^{1/2}, \frac{0.3}{1 + C_{V3} f(C_{kk})\sqrt{L^2}}\right), 1.0\right]. \tag{47}$$

The wall-normal vector, n_i, and the normalized direction of mean vorticity, t_i, are given by Eqs. (13) and (16), respectively.

Conformation tensor transport equation

$$U_k\frac{\partial C_{ij}}{\partial x_k} - M_{ij} - NLT_{ij} = -\frac{1}{\lambda}\left[f(C_{kk})C_{ij} - \delta_{ij}\right], \tag{48}$$

with

$$NLT_{ij} = C_{V1}\frac{\nu_t}{\nu_0}M_{kk}\left(t_i t_j + C_{V2}\frac{v^2}{k}n_i n_j\right). \quad (49)$$

Turbulent kinetic energy transport equation

$$U_j\frac{\partial k}{\partial x_j} = \frac{\partial}{\partial x_j}\left[\left(\nu_s + \frac{\nu_t}{\sigma_k}\right)\frac{\partial k}{\partial x_j}\right] + \left(P_k - \varepsilon^V\right) - \varepsilon, \quad (50)$$

where $P_k = \overline{u_i' u_j'} S_{ij}$ and

$$\varepsilon^V \equiv \varepsilon^V_{kk} = \frac{\nu_p}{2\lambda} f(C_{mm}) NLT_{kk}. \quad (51)$$

Dissipation transport equation

$$U_j\frac{\partial \varepsilon}{\partial x_j} = \frac{\partial}{\partial x_j}\left[\left(\nu_s + \frac{\nu_t}{\sigma_\varepsilon}\right)\frac{\partial \varepsilon}{\partial x_j}\right] + \frac{C_{\varepsilon 1}(P_k - \varepsilon^V) - C_{\varepsilon 2}\varepsilon}{T_t}. \quad (52)$$

Wall normal Reynolds stress transport equation

$$U_j\frac{\partial v^2}{\partial x_j} = \frac{\partial}{\partial x_j}\left[\left(\nu_s + \frac{\nu_t}{\sigma_k}\right)\frac{\partial v^2}{\partial x_j}\right] + kf - \left(6\varepsilon + C_{V2}\varepsilon^V\right)\frac{v^2}{k}. \quad (53)$$

Turbulent redistribution transport equation

$$f - L_t^2\frac{\partial^2 f}{\partial x_j \partial x_j} = \frac{1}{T_t}\left(\frac{2}{3}(C_1 - 1) - (C_1 - 6)\frac{v^2}{k}\right) + \frac{C_2}{1 + C_{V3} f(C_{kk})\sqrt{L^2}}\frac{P_k}{k}. \quad (54)$$

The Newtonian coefficients are given by Pecnik and Iaccarino,[30] and the viscoelastic coefficients are tuned for each system, which are all given in Table II.

V. NUMERICAL PROCEDURE

In order to examine the viscoelastic turbulence model against the DNS data cases within Table I, a finite volume C++ code and configuration case file were developed within OpenFOAM.[60] The computational domain was introduced in the governing equations (Fig. 1). The full domain is reduced based on axial symmetry with a half-channel and one quadrant of the square duct simulated, with a symmetry plane at $y = h \equiv 1$, and $y = z = h \equiv 1$, respectively, where h is the duct half-height. For all cases, the pressure gradient is fixed in the streamwise direction such that $\frac{dP}{dx} \equiv \frac{\Delta P}{\Delta x} = \frac{\langle \tau_w \rangle}{R_h}$, where $\langle \tau_w \rangle$ is the average wall shear stress, $R_h = A_h/P_h$ is the hydraulic radius, A_h is the cross-sectional area of the geometry, and P_h is the "wetted" perimeter. In channel and square duct flows, $R_h = 4h^2/4h = h$ and $R_h = 4h^2/8h = h/2$, respectively.

The non-uniform mesh consists of 75 and 75×75 transverse cells for channel and square duct flow, respectively, with approximately 10 cells located inside the viscous sub-layer. The resultant mesh independence yields mean velocity predictions within 0.1% error for drag reduction predictions, similarly, in Ref. 34.

Many leading DNS studies carried out[9,14,61] require an artificial diffusion term, $\kappa\partial^2 C_{ij}/\partial^2 x_k$, in the transport of C_{ij} to stabilize the sharp near-wall gradients, where κ is an artificial numerical diffusivity constant coefficient. The DNS data apply a value of $\kappa/hu_\tau \sim O(10^{-2})$, which is known to affect mean flow data. A parametric study of a turbulent viscoelastic model found that $\kappa \sim 10^{-3}$–10^{-5} ensures gradients are smoothed out sufficiently to not have large effects on mean velocity calculations.[52] A series of LDR (case 7) simulations are run with ranging κ values $10^{-2} - 10^{-6}$. Table III highlights variations in the magnitude of key field values DR%, U^+_{max}, k^+_{max}, NLT^+_{max}, based on $\kappa\partial^2 C_{mm}/\partial x_k^2$. The results show convergence on $\kappa = 10^{-5}$, which is applied for all resulting simulations in this study. At solid walls, the following boundary conditions are imposed: U_w, k_w, f_w, $v^2_w = 0$; a Neumann condition for $C_{ij,w}$, and P_w; and $\varepsilon_w = 2\nu_s\left(\frac{\partial\sqrt{k}}{\partial x_i}\right)^2$. All cases listed in Table I are run with the Pressure-Implicit with Splitting of Operators (PISO) solver until a steady state is reached (residuals 10^{-5}). The simulations were run on a ASUS ZenBook UX430U laptop with Intel Core i7 processor and 8 GB of RAM, which took roughly 1–5 min to complete a Case.

TABLE II. List of coefficients associated with the Newtonian model, along with the viscoelastic coefficients tuned for channel and square duct flow.

Coefficient	Value
Newtonian:	
C_μ	0.22
σ_k	1.0
σ_ε	1.3
$C_{\varepsilon 1}$	$1.4[1 + 0.045\sqrt{k/\overline{v^2}}]$
$C_{\varepsilon 2}$	1.92
C_1	1.4
C_2	0.3
C_L	0.23
C_η	70.0
Viscoelastic: (Channel/square duct)	
C_{V1}	0.14/0.42
C_{V2}	0.65/0.55
C_{V2}	0.07/0.02

VI. RESULTS AND DISCUSSION

Following the numerical procedure proposed in Sec. V, the model performance is assessed against DNS data for fully developed channel flow and square duct flow as listed in Table I. The model viscoelastic coefficients in Table II are tuned for both channel flow and square duct flow.

A. Fully developed channel flow

The viscoelastic coefficients described in Table II are tuned for cases 7, 10, and 11 in Table I for channel flow to both minimize the

TABLE III. Sensitivity study of κ with LDR (case 7).

K	DR%	U^+_{max}	k^+_{max}	NLT^+_{max}	$\kappa\partial^2 C_{mm}/\partial x_k^2$
10^{-6}	18.26	21.68	4.39	7.96	0.34
10^{-5}	18.26	21.68	4.39	7.96	3.35
10^{-4}	18.14	21.64	4.39	7.95	31.0
10^{-3}	17.01	21.48	4.40	7.75	292
10^{-2}	14.73	21.16	4.51	6.76	1170

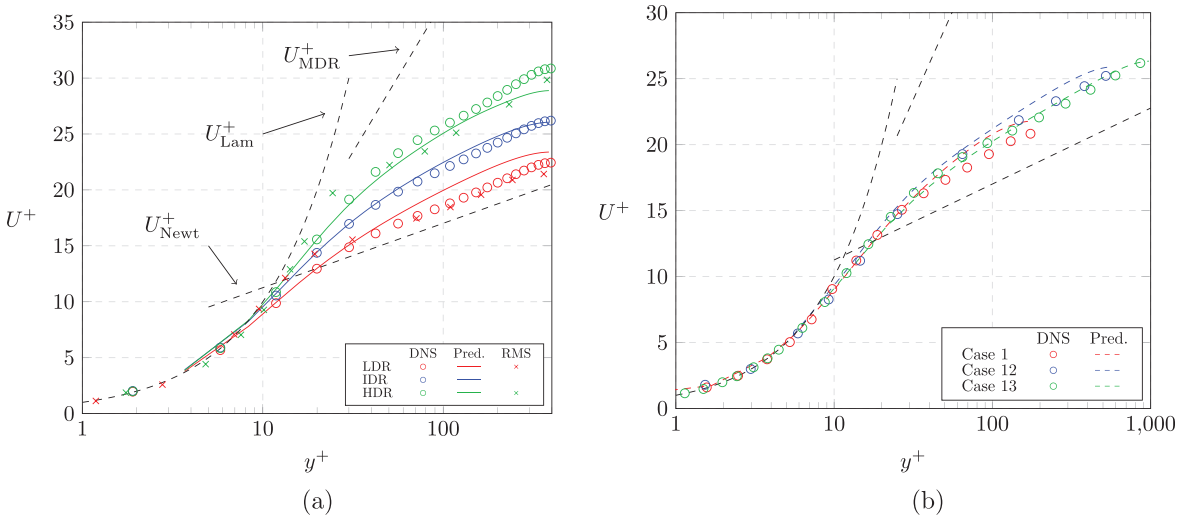

FIG. 6. Transverse profiles of the mean streamwise velocity, U^+: (a) $Re_{\tau_0} = 395$: LDR (case 7), IDR (case 10), and HDR (case 11); (b) $Re_{\tau_0} = 180$, 590, and 1000.

reported DR% and capture polymer-induced flow features. Transverse profiles of the mean streamwise velocity are plotted in Fig. 6, with the corresponding DNS data, current model predictions, and available RSM predictions.[49] The functions labeled are the laminar sub-layer relation, $U^+_{Lam} = y^+$; the Newtonian log-law, $U^+_{Newt} = 2.5\ln(y^+) + 5.5$; and Virk's maximum drag reduction asymptote, $U^+_{MDR} = 11.7\ln(y^+) - 17.0$. In the laminar sub-layer, the velocity profiles collapse on the linear distribution, as they should. Further away from the wall, the mean velocity of LDR, IDR, and HDR increases, with the logarithmic profile shifting upward, captured especially well in the buffer layer where polymers and turbulent vortices predominantly interact. The upward shift of the logarithmic profile can be interpreted as a thickening of the buffer layer in agreement with the experimental and numerical findings of Ptasinski *et al.*[7] and Li *et al.*[9] The current model predictions improve markedly in the buffer layer compared against the RSM study,[49] where they require a damping function within the NLT_{ij} closure model to minimize the over-prediction in this region. The current model also has the capability to predict the mean velocity of various friction Reynolds numbers, from low ($Re_{\tau_0} = 180$) to high ($Re_{\tau_0} = 1000$) as can be viewed in Fig. 6(b).

Figure 7 displays the corresponding model predictions of the root mean square normal Reynolds stresses and Reynolds shear stress, which are compared with the DNS data and available RSM predictions[49] with cases 7, 10, and 11. It is well known that streamwise velocity fluctuations increase slightly with DR, while the transverse, spanwise, and shear components monotonically decrease. Furthermore, the peak locations shift away from the buffer layer which is consistent with the logarithmic layer in the mean velocity profile. The model is in good agreement with the DNS for low, intermediate, and high DR—being capable of capturing the suppression of transverse and spanwise turbulent intensities which is inherent to turbulent DR with dilute polymer solutions. The current model u_{rms} predictions show good improvement compared to the RSM,[49] especially in the buffer layer in which their results predict a large decrease in the streamwise velocity fluctuations. This discrepancy is accounted for in the current model by attenuation of the production term in the pressure–strain. The current model overpredicts LDR and underpredicts HDR slightly for u_{rms}, respectively. It should be noted that this underprediction is arguably somewhat fictitious: in the experiments of Ptasinski *et al.*,[7] u_{rms} increases monotonically for LDR and IDR, with a dip for HDR, but still above the Newtonian line, as shown in the current model predictions. Conversely, their corresponding DNS results over-predict those peak values. Figure 8 displays the transverse profiles for the mean turbulent kinetic energy for low and high friction Reynolds number and DR (cases 1 and 12). The model demonstrates accurate predictions of the general trends observed in the DNS data, surpassing the performance of previous anisotropic models in capturing the increase in the peak of k with increasing viscoelasticity.

Transverse profiles of the mean polymer extension, C_{kk}/L^2, are shown in Fig. 9 for IDR (case 10) and compared against DNS data and the most recent isotropic $v^2 - f$ model[34] for FENE-P fluids. The polymer extension has most physical impact in a region in the buffer layer and inner log layer ($y^+ \sim 30 - 150$), in which the NLT_{kk} term dominates (see Fig. 2). The predictions match well with the DNS and show similarity with the previous model in which the NLT_{kk} term in the current modeling is derived ($NLT_{kk} = C_{V1}\frac{\nu_t}{\nu_0}M_{kk}$).

B. Square duct flow

To assess the performance of the current model against the DNS data in fully developed square duct flow in Table I (cases A and B), the viscoelastic coefficients are first tuned for case 7 in channel flow to calibrate the NLT_{xx} term, and compared against the mean polymer extension and shear stress predictions. Figure 10 displays the transverse profiles of NLT_{xx} and corresponding predictions of C_{xx} and C_{xy}. The peak location and magnitude are captured well for NLT_{xx} against the DNS data in Fig. 10. The effect of the NLT_{xx} predictions for capturing C_{xx} is displayed in Fig. 10(b), which shows a good trend with the DNS

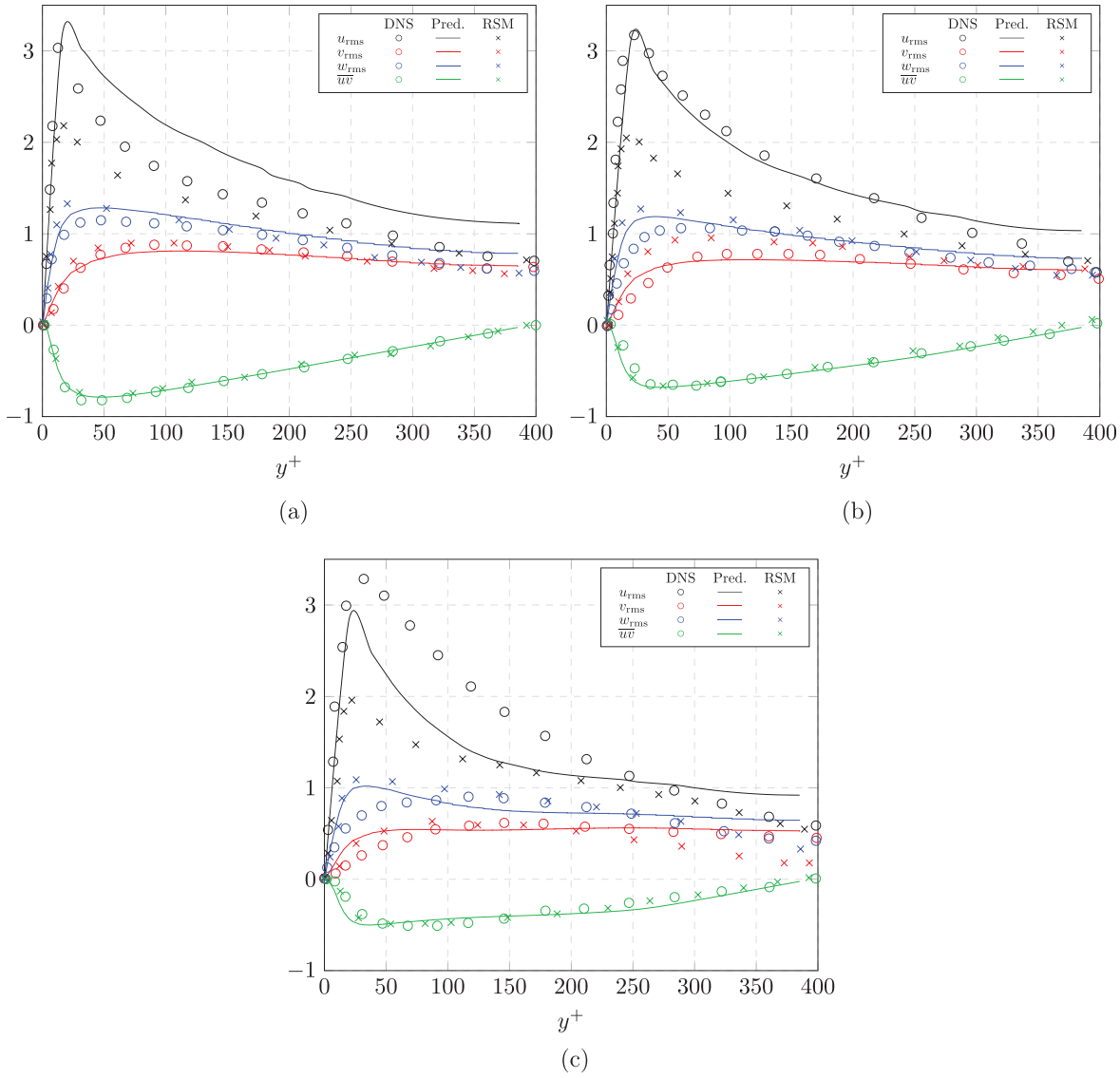

FIG. 7. Transverse profiles of the root mean square normal Reynolds stresses, $\sqrt{\overline{u_i' u_i'}}$, and Reynolds shear stress, $\overline{u'v'}$: (a) LDR (case 7), (b) IDR (case 10), and (c) HDR (case 11).

data. The C_{xy} component depends on NLT_{xx} predictions with a v^2/k scale, also displaying a good general trend with the DNS data.

Figure 11 displays the y–z plane contour profiles of NLT_{xx} and $NLT_{v^2} = NLT_{yy} + NLT_{zz}$ for case B. There is a symmetry exhibited about the $y = z$ line for both fields, as it should, owing to the complete NLT_{ij} closure model. The magnitude of NLT_{xx} in the square duct peaks along the central line, $y = z = 1$, at a similar location consistent with channel flow data in Fig. 10. The peak and mean values decrease consistently, with a small second peak $y/h = 0.4$, as the duct corner is approached. This behavior is concurrent with the turbulent shearing activity or wall shear stress in the DNS findings.[20]

The NLT_{v^2} term maintains a similar structure to the NLT_{xx} term but with a shifts away from the wall, where polymer shear is most active, along with a reduced magnitude of about 10 owing to the v^2/k scaling.

Figure 12 displays transverse profiles of the mean streamwise conformation tensor, C_{xx}, at various locations along the z-axis: $z/h = 1$, 0.7, and 0.4. The predictions against the DNS data at the centerline ($z/h = 1$) are similar to those exhibited within channel flow as discussed previously. Away from the centerline, for cases $z/h = 0.7$ and 0.4, there is a shift of the mean value of $C_{xx}(\sim 200)$ which moves closer to the wall, at locations $y/h \sim 0.35$ and $y/h \sim 0.2$, respectively.

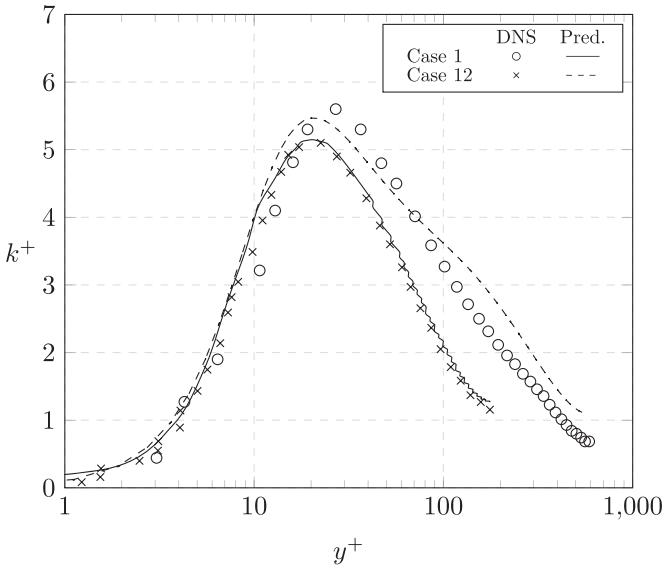

FIG. 8. Transverse profiles of the mean turbulent kinetic energy, k^+.

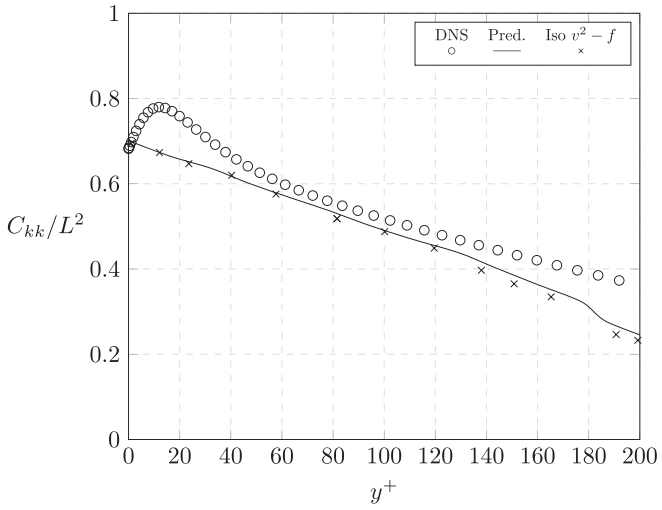

FIG. 9. Transverse profiles of the mean polymer extension, C_{kk}/L^2, for IDR (case 10), compared with the most recent isotropic v^2-f model.

The behavior for $z/h = 0.4$ also exhibits an increased near-wall and centerline peak. The overall trends are captured well with the DNS, which is a direct result of the NLT_{xx} modeling and results previously discussed from Fig. 11.

Figure 13 displays the y–z contour profiles of the in-plane velocity $\tilde{V}^+ = \sqrt{(V^+)^2 + (W^+)^2}$, and mean streamwise velocity U^+, for Newtonian flow and case B. Figures 13(a) and 13(b) have the in-plane velocity vectors imposed for $\tilde{V}^+$, and the bottom panels show additional white contour lines on U^+ for improved visuals. On the centerline ($z/h = 1$), there is a shift in the mean velocity logarithmic profile from Newtonian to polymeric flow, which is consistent with the channel flow predictions. The polymeric flow exhibits bending of the mean velocity contour lines, with a shift away from the wall near the centerline, and a shift toward the wall near the duct corner, which can be visualized with the gray arrows in Fig. 13(d). The in-plane velocity magnitudes, $\tilde{V}^+$ increase from Newtonian to polymeric flow, especially along the symmetry line $y = z$ and in the near wall regions ($z/h \sim 0.05$). The locations of the mean streamwise vorticity, marked with a dot in Figs. 13(a) and 13(b), move further away from the walls and displacing toward the center. This behavior is concurrent with the DNS findings[20] for turbulent polymeric square duct flow and are a result of the current modeling of second normal Reynolds stress differences from the polymer-induced flow. To compare quantitatively with the available DNS data, Fig. 14 displays the transverse profiles of U^+ along locations along the z axis at different locations: $z = 1$, 0.7, and

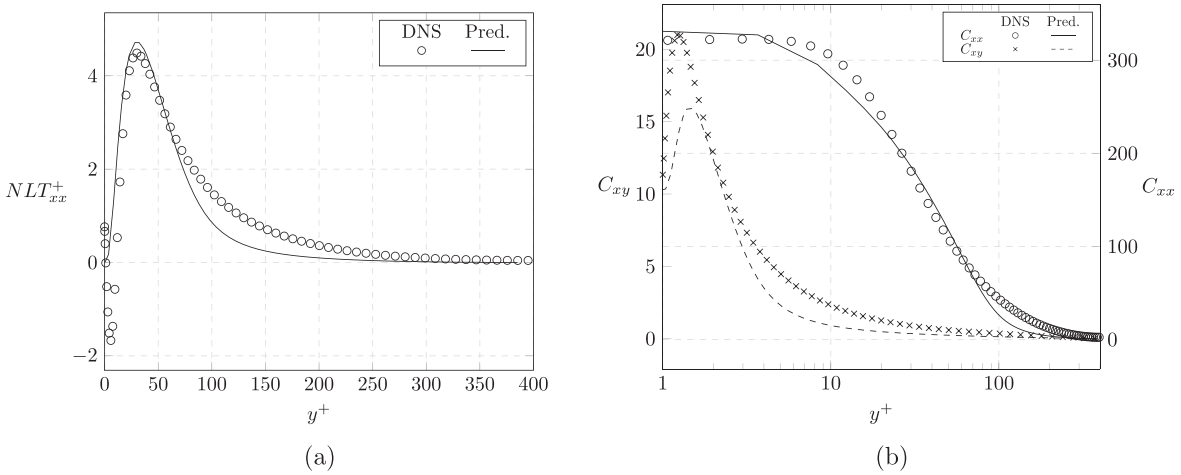

FIG. 10. Transverse profiles of (a) NLT^+_{xx} and (b) C_{xx} and C_{xy} for LDR (case 7).

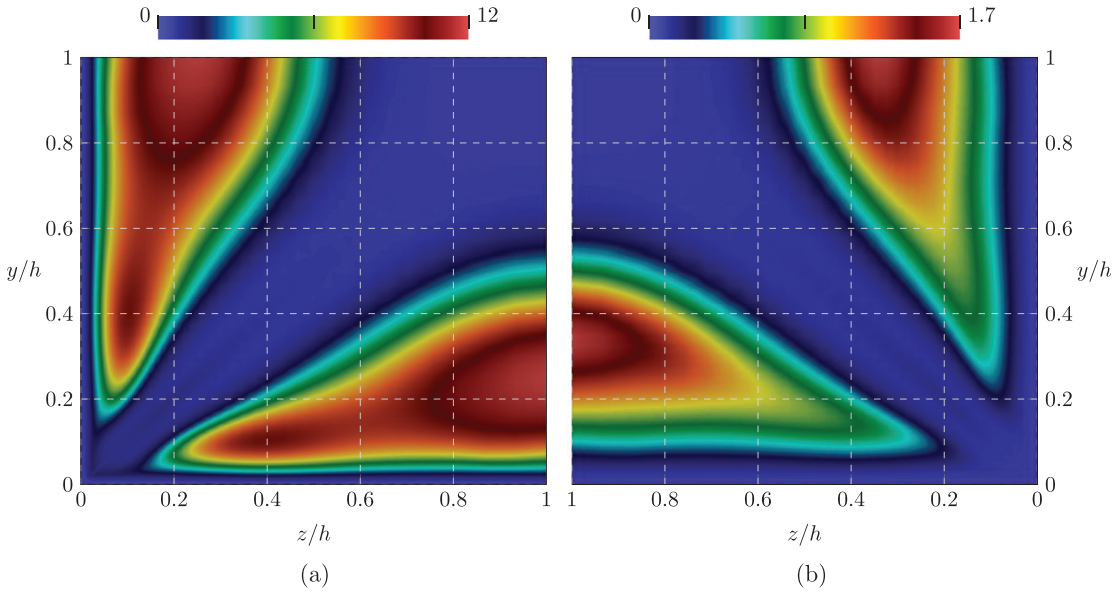

FIG. 11. Contour profiles of (a) NLT^{+}_{xx} and (b) $NLT^{+}_{v^2}$, in square duct flow (case B).

0.4, similarly with previous figures. The model performs well against the DNS data capturing the shift away from the buffer layer, whilst also featuring the drop in magnitude for $z = 0.4$ at the centerline, owing to the effects of secondary flow on mean flow previously discussed.

Figure 15 displays the mean local normalized wall shear stress, $\bar{\tau}_w/\langle\tau_w\rangle$, along the wall ($y = 0$) for Newtonian flow and case B. There is an increase in the near-wall vicinity and decrease near the centerline for $\bar{\tau}_w/\langle\tau_w\rangle$ from Newtonian to polymeric flow, which matches well with the DNS data. This is a result of the varying secondary flow features and shift in the vorticity away from the wall, as discussed previously and can be visualized by the gray arrows in Fig. 13(d).

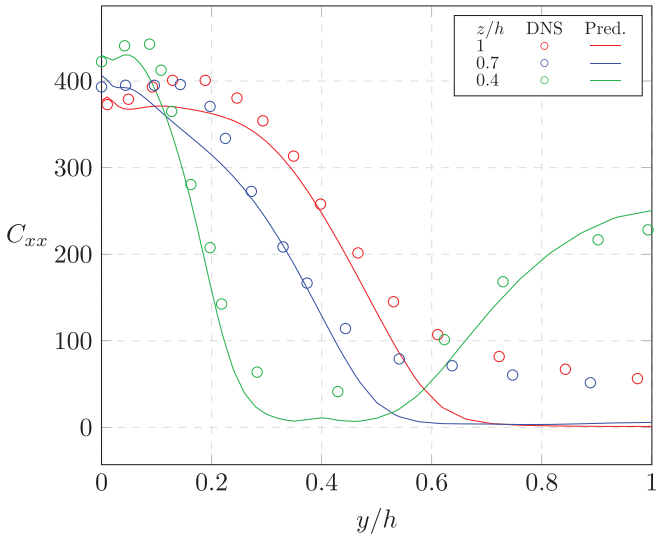

FIG. 12. Transverse profiles of the mean streamwise conformation tensor, C_{xx}, in square duct flow (case B) along locations of the z axis.

VII. CONCLUSION

The main conclusions of this work are summarized below:

(1) A novel open-source anisotropic $k - \varepsilon - v^2 - f$ model is presented for turbulent viscoelastic duct flow with dilute polymeric solutions described by the FENE-P constitutive model. The turbulence model for channel and square duct flow of Newtonian fluids[30] is adapted to incorporate the polymeric terms within the governing equations. The non-linear terms that require closure are developed with simple and sophisticated models based on *a priori* analysis with independent DNS data in fully developed channel flow at friction Reynolds number $Re_{\tau_0} = 395$, for low, intermediate, and high drag reduction.

(2) The NLT_{ij} term, which accounts for the interaction between fluctuating components of the conformation tensor and the velocity gradient tensor, is newly modeled with the mean flow direction, t_i, and wall-normal, n_i, present in the Newtonian model. This is based on the natural streamwise alignment of the mean polymer stretch and the transverse component primarily responsible for polymer shear. The implicit polymer effects on pressure–strain increase the magnitude of the streamwise Reynolds stress component, which is assessed with a simple *ad hoc* closure accounting for the reduced near-wall production of turbulent kinetic energy. The same closure model is adapted for the span-wise Reynolds stress for predictions of polymer-enhanced secondary flow via second normal stress differences.

(3) The model performs well against DNS data in channel flow from low to high friction Reynolds numbers ($Re_{\tau_0} = 180 - 1000$) with a range of rheological parameters

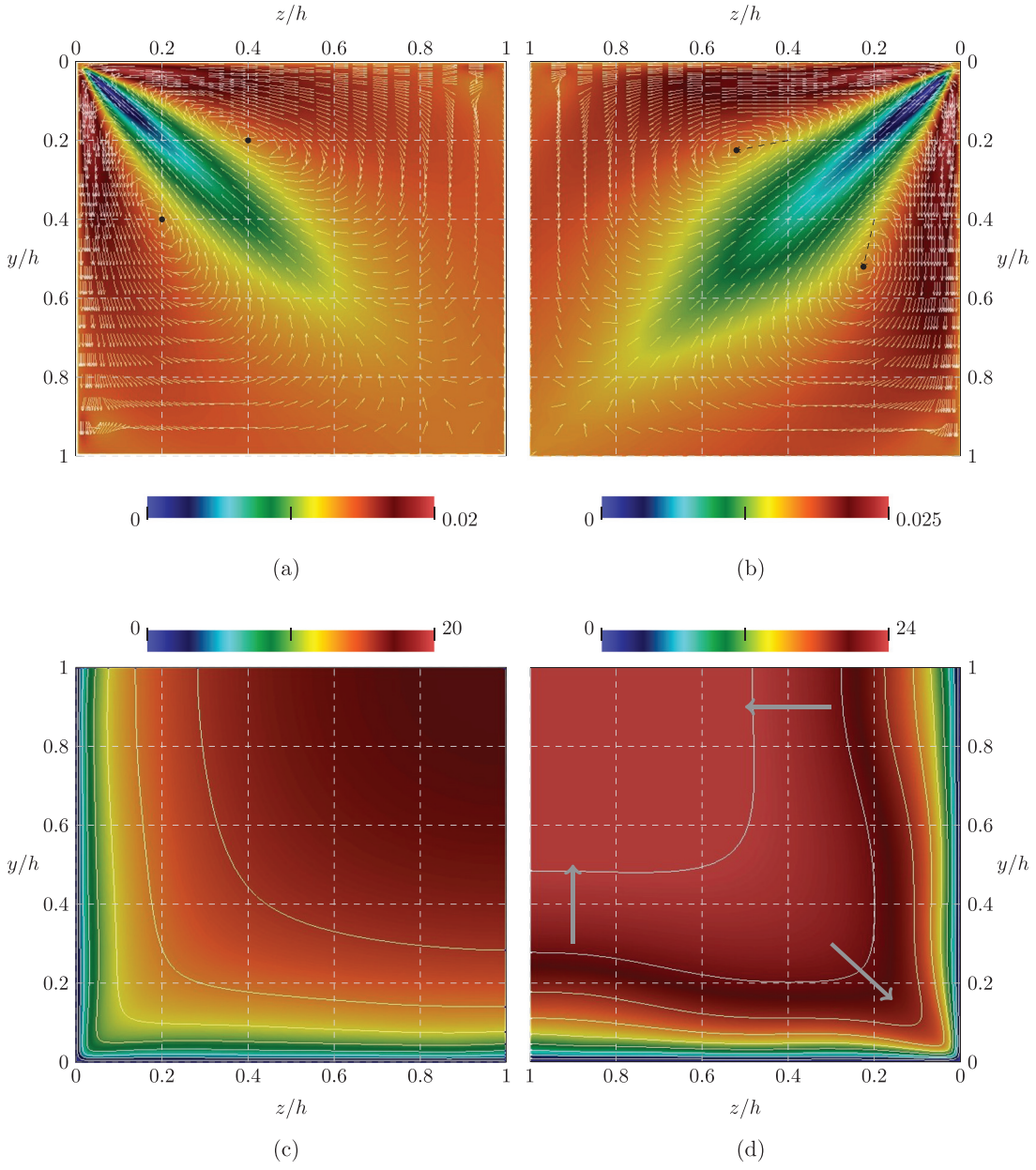

FIG. 13. Contour profiles of (a) and (b) in-plane velocity $\tilde{V}^+$ with velocity vectors imposed, and (c) and (d) mean streamwise velocity U^+ with white contour lines at spacing $U^+/25$ for improved visuals. (a) and (c) Newtonian and (b) and (d) case B. The gray arrows in (d) are to visualize the warped isolines for polymeric flow.

($Wi_{\tau_0} = 25 - 1000$, $L^2 = 900 - 3600$, $\beta = 0.9$) and captures low, intermediate, and high drag reduced flow features—including mean streamwise velocity, Reynolds shear stress and all normal stresses (or turbulent kinetic energy), and the conformation tensor field. The model capabilities are extended for square ducts (or any regular polygon) due to the symmetric modeling of the closures, which can predict the mean streamwise velocity, secondary flow features associated with second normal Reynolds stress differences, the spatial variation of the conformation tensor field, and mean wall shear stress, against DNS data at intermediate friction Reynolds number and drag reduction ($Re_{\tau_0} = 366$, $L^2 = 900$, $Wi_{\tau_0} = 36$).

(4) The model does not contain any dependence on friction velocity (e.g., Wi_{τ_0}), which is important to avoid flow stagnation or code instability. The simple closure models adapted and numerically inexpensive method are advantageous for further

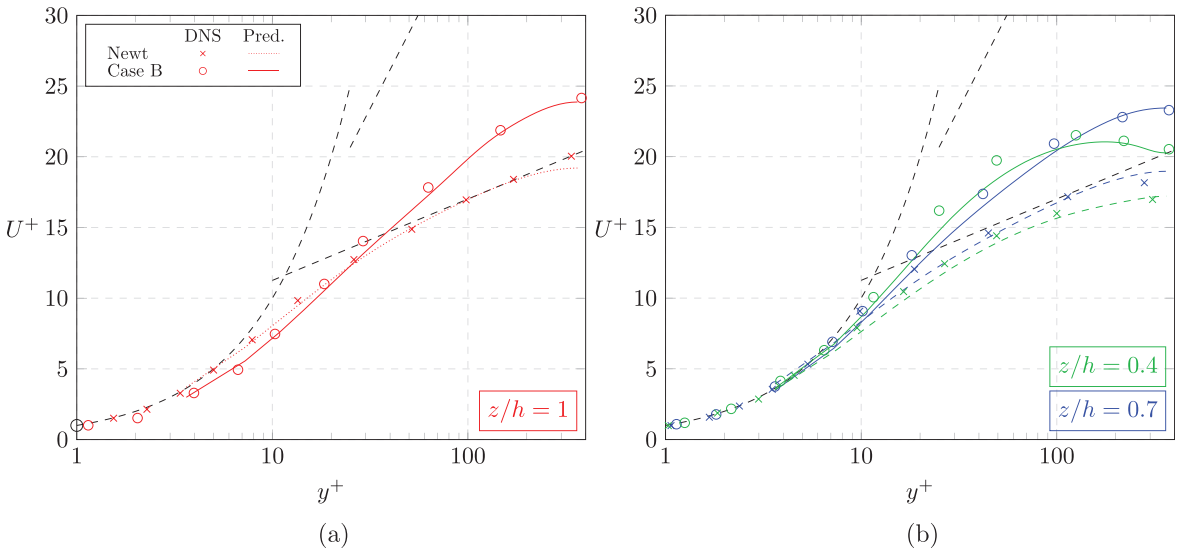

FIG. 14. Transverse profiles of the mean streamwise velocity, U^+, in square duct flow (Newtonian and case B) along locations of the z axis. The black dotted lines are theory lines as shown in Fig. 6. (a) $z/h = 1$ and (b) $z/h = 0.4$ and 0.7.

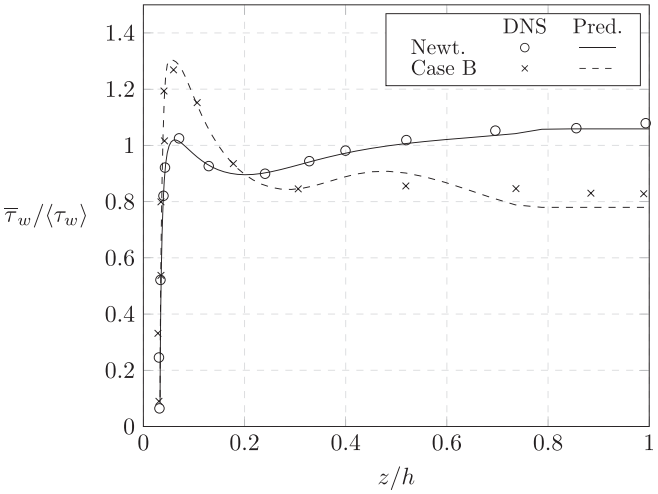

FIG. 15. Profile along the wall ($y = 0$) of the mean local normalized wall shear stress, $\overline{\tau}_w/\langle\tau_w\rangle$, in square duct flow (Newtonian and case B).

developments of 3D codes in more complex geometries. Accessible codes and models are crucial for the advancement and improvement of turbulent viscoelastic models, and an OpenFOAM C++ code package is developed and freely available on GitHub.

ACKNOWLEDGMENTS

Financial support during the Ph.D. studentship from the Engineering and Physical Sciences Research Council (EPSRC) (Grant No. EP/N5059681/1, Award Reference: 1958044] was greatly acknowledged by M. McDermott.

AUTHOR DECLARATIONS

Conflict of Interest

The authors have no conflicts to disclose.

Author Contributions

Michael McDermott: Conceptualization (lead); Data curation (lead); Formal analysis (lead); Investigation (lead); Methodology (lead); Project administration (equal); Resources (equal); Software (lead); Validation (lead); Visualization (equal); Writing – original draft (lead); Writing – review & editing (lead). **Theo Riou:** Conceptualization (equal); Data curation (equal); Formal analysis (equal); Investigation (equal); Methodology (supporting); Resources (supporting); Software (equal); Validation (equal); Visualization (equal). **Pedro Resende:** Conceptualization (equal); Data curation (supporting); Formal analysis (supporting); Investigation (supporting); Methodology (supporting); Project administration (supporting); Resources (supporting); Software (supporting); Supervision (equal); Writing – review & editing (equal). **Mark C. T. Wilson:** Conceptualization (equal); Data curation (supporting); Funding acquisition (equal); Investigation (supporting); Methodology (supporting); Project administration (equal); Resources (supporting); Software (supporting); Supervision (equal); Writing – review & editing (supporting). **Alexandre Afonso:** Conceptualization (equal); Data curation (supporting); Formal analysis (supporting); Investigation (supporting); Methodology (equal); Project administration (supporting); Resources (supporting); Software (equal); Supervision (supporting); Writing – review & editing (supporting). **Gregory Nicholas de Boer:** Conceptualization (equal); Data curation (supporting); Formal analysis (equal); Funding acquisition (equal); Investigation (equal); Methodology (equal); Project administration (equal); Resources (equal); Software (equal); Supervision (lead); Validation (equal); Visualization (equal); Writing – review & editing (equal).

DATA AVAILABILITY

The data that support the findings of this study are available from the corresponding author upon reasonable request.

REFERENCES

[1]B. Toms, "Some observations on the flow of linear polymer solutions through straight tubes at large Reynolds numbers," in *Proceedings of 1st International Congress on Rheology* (North-Holland Publishing Company, 1948), p. 135.
[2]J. W. Lumley, "Drag reduction by additives," Annu. Rev. Fluid Mech. **1**, 367–384 (1969).
[3]J. W. Hoyt, "Turbulent flow of drag-reducing suspensions," Technical Report No. NUC-TP-299 (Naval Undersea Center, San Diego, CA, 1972).
[4]P. S. Virk, E. W. Merrill, H. S. Mickley, K. A. Smith, and E. L. Mollo-Christensen, "The Toms phenomenon: Turbulent pipe flow of dilute polymer solutions," J. Fluid Mech. **30**, 305–328 (1967).
[5]P. S. Virk, "Drag reduction fundamentals," AIChE J. **21**, 625–656 (1975).
[6]C. D. Dimitropoulos, R. Sureshkumar, A. N. Beris, and R. A. Handler, "Budgets of Reynolds stress, kinetic energy and streamwise enstrophy in viscoelastic turbulent channel flow," Phys. Fluids **13**, 1016–1027 (2001).
[7]P. K. Ptasinski, B. J. Boersma, F. T. M. Nieuwstadt, M. A. Hulsen, B. H. A. A. V. den Brule, and J. C. R. Hunt, "Turbulent channel flow near maximum drag reduction: Simulations, experiments and mechanisms," J. Fluid Mech. **490**, 251–291 (2003).
[8]Y. Dubief, V. E. Terrapon, C. M. White, E. S. G. Shaqfeh, P. Moin, and S. K. Lele, "New answers on the interaction between polymers and vortices in turbulent flows," Flow, Turbul. Combust. **74**, 311–329 (2005).
[9]C. F. Li, R. Sureshkumar, and B. Khomami, "Influence of rheological parameters on polymer induced turbulent drag reduction," J. Non-Newtonian Fluid Mech. **140**, 23–40 (2006).
[10]L. Thais, T. B. Gatski, and G. Mompean, "Some dynamical features of the turbulent flow of a viscoelastic fluid for reduced drag," J. Turbul. **13**, N19 (2012).
[11]C. M. White and M. G. Mungal, "Mechanics and prediction of turbulent drag reduction with polymer additives," Annu. Rev. Fluid Mech. **40**, 235–256 (2008).
[12]L. Xi, "Turbulent drag reduction by polymer additives: Fundamentals and recent advances," Phys. Fluids **31**, 121302 (2019).
[13]R. B. Bird, P. J. Dotson, and N. L. Johnson, "Polymer solution rheology based on a finitely extensible bead–spring chain model," J. Non-Newtonian Fluid Mech. **7**, 213–235 (1980).
[14]K. Kim, C. F. Li, R. Sureshkumar, S. Balachandar, and R. J. Adrian, "Effects of polymer stresses on eddy structures in drag-reduced turbulent channel flow," J. Fluid Mech. **584**, 281–299 (2007).
[15]M. Masoudian, K. Kim, F. T. Pinho, and R. Sureshkumar, "A viscoelastic $k-\varepsilon-v^2-f$ turbulent flow model valid up to the maximum drag reduction limit," J. Non-Newtonian Fluid Mech. **202**, 99–111 (2013).
[16]L. Thais, T. B. Gatski, and G. Mompean, "Analysis of polymer drag reduction mechanisms from energy budgets," Int. J. Heat Fluid Flow **43**, 52–61 (2013).
[17]M. C. Guimarães, N. Pimentel, F. T. Pinho, and C. B. da Silva, "Direct numerical simulations of turbulent viscoelastic jets," J. Fluid Mech. **899**, A11 (2020).
[18]M. C. Guimarães, P. T. Pinho, and C. B. da Silva, "Turbulent planar wakes of viscoelastic fluids analysed by direct numerical simulations," J. Fluid Mech. **946**, A26 (2022).
[19]M. E. Rosti and L. Brandt, "Increase of turbulent drag by polymers in particle suspensions," Phys. Rev. Fluids **5**, 041301 (2020).
[20]A. Shahmardi, S. Zade, M. N. Ardekani, R. J. Poole, F. Lundell, M. E. Rosti, and L. Brandt, "Turbulent duct flow with polymers," J. Fluid Mech. **859**, 1057–1083 (2019).
[21]N. V. Nikitin, N. V. Popelenskaya, and A. Stroh, "Prandtl's secondary flows of the second kind. problems of description, prediction, and simulation," Fluid Dyn. **56**, 513–538 (2021).
[22]L. C. Hoagland, "Fully developed turbulent flow in straight rectangular ducts: Secondary flow, its cause and effect on the primary flow," Ph.D. thesis (Massachusetts Institute of Technology, 1962).
[23]J. Nikuradse, "Untersuchungen über turbulente strömungen in nicht kreisförmigen rohren," Ing.-Arch. **1**, 306–332 (1930).
[24]H. J. Leutheusser, "Turbulent flow in rectangular ducts," J. Hydraul. Div. **89**, 1–19 (1963).
[25]H. Abreu, F. T. Pinho, and C. B. da Silva, "Turbulent entrainment in viscoelastic fluids," J. Fluid Mech. **934**, A36 (2022).
[26]C. G. Speziale, "On turbulent secondary flows in pipes of non-circular cross-section," Int. J. Eng. Sci. **20**, 863–872 (1982).
[27]C. G. Speziale, "On nonlinear k – l and $k-\varepsilon$ models of turbulence," J. Fluid Mech. **178**, 459–475 (1987).
[28]S. Nisizima, "A numerical study of turbulent square-duct flow using an anisotropic $k-\varepsilon$ model," Theor. Comput. Fluid Dyn. **2**, 61–71 (1990).
[29]S. B. Pope, "A more general effective-viscosity hypothesis," J. Fluid Mech. **72**, 331–340 (1975).
[30]R. Pecnik and G. Iaccarino, "Predictions of turbulent secondary flows using the v^2-f model," AIAA Paper No. 2008-3852, 2008.
[31]F. S. Lien, G. Kalitzin, and P. A. Durbin, "RANS modelling for compressible and transitional flows," in *Summer Program Centre for Turbulence Research* (Stanford, 1998), pp. 267–286.
[32]D. Modesti, "A priori tests of eddy viscosity models in square duct flow," Theor. Comput. Fluid Dyn. **34**, 713–734 (2020).
[33]D. R. Laurence, J. C. Uribe, and S. V. Utyuzhnikov, "A robust formulation of the v^2-f model," Flow, Turbul. Combust. **73**, 169–185 (2005).
[34]M. Masoudian, F. T. Pinho, K. Kim, and R. Sureshkumar, "A RANS model for heat transfer reduction in viscoelastic turbulent flow," Int. J. Heat Mass Transfer **100**, 332–346 (2016).
[35]R. Leighton, D. T. Walker, T. Stephens, and G. Garwood, "Reynolds stress modelling for drag-reducing viscoelastic flows," in *Proceedings of 4th Joint Fluids Summer Engineering Conference* (ASME, 2003), pp. 735–744.
[36]K. D. Housiadas and A. N. Beris, "Characteristic scales and drag reduction evaluation in turbulent channel flow of non-constant viscosity viscoelastic fluids," Phys. Fluids **16**, 1581–1586 (2004).
[37]F. T. Pinho, C. F. Li, B. A. Younis, and R. Sureshkumar, "A low Reynolds number turbulence closure for viscoelastic fluids," J. Non-Newtonian Fluid Mech. **154**, 89–108 (2008).
[38]C. F. Li, V. K. Gupta, R. Sureshkumar, and B. Khomami, "Turbulent channel flow of dilute polymeric solutions: Drag reduction scaling and an eddy viscosity model," J. Non-Newtonian Fluid Mech. **139**, 177–189 (2006).
[39]P. R. Resende, K. Kim, B. A. Younis, R. Sureshkumar, and F. T. Pinho, "A FENE-P $k-\varepsilon$ turbulence model for low and intermediate regimes of polymer-induced drag reduction," J. Non-Newtonian Fluid Mech. **166**, 639–660 (2011).
[40]P. R. Resende, K. Kim, B. A. Younis, R. Sureshkumar, and F. T. Pinho, "Development of a low-Reynolds-number $k-\omega$ model for FENE-P fluids," Flow, Turbul. Combust. **90**, 69–94 (2013).
[41]P. R. Resende, A. M. Afonso, and D. O. Cruz, "An improved $k-\varepsilon$ turbulence model for FENE-P fluids capable to reach high drag reduction regime," Int. J. Heat Fluid Flow **73**, 30–41 (2018).
[42]P. R. Resende, F. T. Pinho, and P. J. Oliveira, "Improvement of the energy distribution in isotropic turbulent viscoelastic fluid models," in *Proceedings of MEFTE*, Porto, Portugal, 11-12 September 2014, pp. 221–226.
[43]P. R. Resende and A. S. Cavadas, "New developments in isotropic turbulent models for FENE-P fluids," Fluid Dyn. Res. **50**, 025508 (2018).
[44]M. McDermott, P. R. Resende, T. Charpentier, M. Wilson, A. Afonso, D. Harbottle, and G. de Boer, "A FENE-P $k-\varepsilon$ viscoelastic turbulence model valid up to high drag reduction without friction velocity dependence," Appl. Sci. **10**, 8140 (2020).
[45]M. McDermott, P. R. Resende, T. Charpentier, M. Wilson, A. Afonso, D. Harbottle, and G. de Boer, "An improved $k-\omega$ turbulence model for FENE-P fluids without friction velocity dependence," Int. J. Heat Fluid Flow **90**, 108799 (2021).
[46]G. Iaccarino, E. S. G. Shaqfeh, and Y. Dubief, "Reynolds-averaged modelling of polymer drag reduction in turbulent flows," J. Non-Newtonian Fluid Mech. **165**, 376–384 (2010).
[47]F. T. Pinho, B. Sadanandan, and R. Sureshkumar, "One equation model for turbulent channel flow with second order viscoelastic corrections," Flow, Turbul. Combust. **81**, 337–367 (2008).
[48]R. Benzi, "A short review on drag reduction by polymers in wall bounded turbulence," Phys. D **239**, 1338–1345 (2010).

[49]M. Masoudian, K. Kim, F. T. Pinho, and R. Sureshkumar, "A Reynolds stress model for turbulent flow of homogeneous polymer solutions," Int. J. Heat Fluid Flow **54**, 220–235 (2015).
[50]P. R. Resende, F. T. Pinho, and D. O. Cruz, "A Reynolds stress model for turbulent flows of viscoelastic fluids," J. Turbul. **14**, 1–36 (2013).
[51]Z. Y. Zheng, F. Li, and Q. Li, "Reynolds-averaged simulation on turbulent drag-reducing flows of viscoelastic fluid based on user-defined function in FLUENT package," in *Proceedings of 12th International Conference on Nanochannels, Microchannels, and Minichannels* (ASME, 2014), p. V01AT03A010.
[52]S. Azad, A. Riasi, and H. A. Moghadam, "Parametric study of a viscoelastic RANS turbulence model in the fully developed channel flow," J. Comput. Appl. Mech. **48**, 65–74 (2017).
[53]M. A. Alves, P. J. Oliveira, and F. T. Pinho, "Numerical methods for viscoelastic fluid flows," Annu. Rev. Fluid Mech. **53**, 509–541 (2021).
[54]K. D. Housiadas, A. N. Beris, and R. A. Handler, "Viscoelastic effects on higher order statistics and on coherent structures in turbulent channel flow," Phys. Fluids **17**, 035106 (2005).
[55]P. Tucker, "Prediction of turbulent oscillatory flows in complex systems," Int. J. Numer. Methods Fluids **33**, 869–895 (2000).
[56]R. Moser, J. Kim, and N. Mansour, "Direct numerical simulation of turbulent channel flow up to $Re_{\tau_0} = 590$," Phys. Fluids **11**, 943–945 (1999).
[57]R. Manceau, M. Wang, and P. Durbin, "Assessment of non-local effect on pressure term in RANS modeling using a DNS database," in *Proceedings of Summer Program* (Stanford, 1998), pp. 303–322.
[58]R. Manceau and K. Hanjalić, "A new form of the elliptic relaxation equation to account for wall effects in RANS modeling," Phys. Fluids **12**, 2345–2351 (2000).
[59]Y. Dubief, G. G. Laccarino, and S. K. Lele, "A turbulence model for polymer flows," in *Center for Turbulence Research* (Stanford, 2004), pp. 63–72.
[60]M. McDermott, "RANS turbulence models for FENE-P viscoelastic fluids," Ph.D. thesis (University of Leeds, 2022).
[61]R. Sureshkumar, A. N. Beris, and R. A. Handler, "Direct numerical simulation of the turbulent channel flow of a polymer solution," Phys. Fluids **9**, 743–755 (1997).